STUDIES OF MIXED-PHASE CLOUD MICROPHYSICS USING AN IN-SITU UNMANNED AERIAL VEHICLE (UAV) PLATFORM

A Thesis
Presented to
The Academic Faculty

By

Robyn D. Williams

In Partial Fulfillment
Of the Requirements for the Degree
Master of Science in the
School of Chemical and Biomolecular Engineering

Georgia Institute of Technology
August 2005

STUDIES OF MIXED-PHASE CLOUD MICROPHYSICS USING AN IN-SITU UNMANNED AERIAL VEHICLE (UAV) PLATFORM

Approved by:

Dr. Athanasios Nenes, Advisor
School of Chemical and Biomolecular Engineering
School of Earth and Atmospheric Sciences
Georgia Institute of Technology

Dr. Judith Curry
School of Atmospheric Sciences
Georgia Institute of Technology

Dr. Amyn Teja
School of Chemical and Biomolecular Engineering
Georgia Institute of Technology

Date Approved: July 12, 2005

ACKNOWLEDGEMENT

First and foremost, I would like to thank God for being faithful and providing strength and peace throughout my entire graduate school career and thesis process. All of my strength comes from the Lord!

*Psalms 28:*6-7 (Contemporary English Version)

I praise you, Lord, for answering my prayers. You are my strong shield, and I trust you completely. You have helped me, and I will celebrate and thank you in song.

I would like to thank my entire family and friends for all of their prayers, encouraging words, and support. I especially would like to thank my parents, Mr. & Mrs. Robert and Dian Williams, for being the best parents in the world by supporting me in every way – emotionally, spiritually, physically, and financially!!! I would like to thank my thesis coach, Ms. Crystal Gilpin. Thanks for making sure I stayed on schedule, helping me to re-focus during my overwhelming moments, and most of all reading through my thesis drafts. All of you were very instrumental in my graduate school success.

Thanks to my advisor, Dr. Athanasios Nenes, for his guidance, assistance, patience, and support throughout my graduate school career. I would also like to thank my research group for their support and assistance.

Thanks to Dr. James Pinto for providing the mini-VIPS data from the Aerosonde flight and for assisting with the image processing. Thanks to Dr. Judith Curry and Dr. Amyn Teja for serving on my thesis committee and providing feedback on my thesis.

This work was financially supported by the National Science Foundation grants DGE-0086420 and DGE-0338261 through the Georgia Tech Student Teacher Enhancement Partnership Fellowship Program and Georgia Tech Faculty Startup funds

TABLE OF CONTENTS

LIST OF TABLES

LIST OF FIGURES

LIST OF SYMBOLS AND ACRONYMS

2D-C: Two Dimensional Cloud Probe

A: Habit dependent constant from mass-length relationships

$A_{p:}$ Particle Area (cm^2/L)

A_r: Area Ratio (dimensionless)

A_s: Surface Area (cm^2/L)

A_T: Total Area (cm^2/L)

AMS: American Meteorological Society

ARM: Atmospheric Radiation Measurement

b: Coefficient in Kohler equation

B: Habit dependent constant in mass-length relationships

C: Particle concentration (#/L)/s

CART: Cloud and Radiation Testbed

CCN: Cloud Condensation Nuclei

CEPEX: Central Equatorial Pacific Experiment

CRYSTAL-FACE: Cirrus Regional Study of Tropical Anvils Cirrus Layers-Florida Area Cirrus Experiment

CVI: Counterflow Virtual Impactor

d: distance between two locations (km)

$D_A^{'}$: Modified diffusivity constant

DMS: Dimethylsulfide

DOE: Department of Energy

D_p: Particle Diameter, μm

$\overline{D_p}$: Mean particle diameter

F: Fraction of particles with habit j

FIRE: First ISSCP Regional Experiment

FIRE-ACE: First ISSCP Regional Experiment – Arctic Cloud Experiment

fs: speed of the film (s)

FSSP: Forward Scattering Spectral Probe

GPS: Global Positioning System

IDL: interactive data language

IFO: Intensive Field Operations

IN: Ice Nuclei

IPCC: International Panel on Climate Change

ISSCP: First International Satellite Cloud Climate Climatology Project

IWC: ice water content

l_p: Length of particle

L_i: Crystal Length

MMCR: millimeter-wavelength cloud radar

MODIS: Moderate Resolution Imaging Spectroradiometer

M_w: Molecular weight of water

N: Number concentrations, cm^{-3}

n_i: Number concentration per size bin i ($\#/m^3$)

n_p: Number of pixels (count)

n_r: Number of regions in mini-VIPS frame

n_s: Solute moles

NCAR: National Center for Atmospheric Research

NOAA: National Oceanic and Atmospheric Administration

n_p: number of pixels (dimensionless/count)

PVM: Particulate Volume Monitor (PVM)

ps: Pixel size (cm)

r_l: Radius of aqueous solution drop

S_a: Air speed (cm/s)

S_c: Critical saturation

S_f: Speed of film (mm/s)

SHEBA: Surface Heat Budget of the Artic Ocean experiment

t_e: Time the film is exposed to the air (s)

UAV: Unmanned Aerial Vehicles

UTC: Universal Time Coordinates

VIPS: Video Ice Particle Sampler

V_s: Sample volume (l/s)

w_s: Width of the slit

ε: Extinction (km^{-1})

λ: Latitude in radians

Λ: Longitude in radians

ρ_w: Density of water

σ: Standard deviation

σ_l: Fractional environmental water super saturation

σ_p: Pixel size (cm)

σ_w: Air-water surface tension

SUMMARY

Cirrus clouds cover between 20% - 50% of the globe and are an essential component in the climate. The improved understanding of ice cloud microphysical properties is contingent on acquiring and analyzing in-situ and remote sensing data from cirrus clouds. In –situ observations of microphysical properties of ice and mixed-phase clouds using the mini-Video Ice Particle Sizer (mini-VIPS) aboard robotic unmanned aerial vehicles (UAVs) provide a promising and powerful platform for obtaining valuable data in a cost-effective, safe, and long-term manner.

The purpose of this study is to better understand cirrus microphysical properties by analyzing the effectiveness of the mini-VIPS/UAV in-situ platform. The specific goals include:

(1) To validate the mini-VIPS performance by comparing the mini-VIPS data retrieved during an Artic UAV mission with data retrieved from the millimeter-wavelength cloud radar (MMCR) at the Barrow ARM/CART site.

(2) To analyze mini-VIPS data to survey the properties of high latitude mixed-phase clouds

The intercomparison between in-situ and remote sensing measurements was carried out by comparing reflectivity values calculated from in-situ measurements with observations from the MMCR facility. Good agreement between observations and measurements is obtained during the time frame where the sampled volume was saturated with respect to ice. We also have

shown that the degree of closure between calculated and observed reflectivity strongly correlates with the assumption of ice crystal geometry observed in the mini-VIPS images. The good correlation increases the confidence in mini-VIPS and MMCR measurements. Finally, the size distribution and ice crystal geometry obtained from the data analysis is consistent with published literature for similar conditions of temperature and ice supersaturation.

CHAPTER 1

INTRODUCTION

1.1 BACKGROUND[AN1]

The climate is a very sensitive and integrated system. The effect of interactions between aerosols (i.e. suspended particulate material) and clouds on the climate is one of the largest sources of uncertainty in the fields of the atmospheric sciences. Aerosol concentration, composition, and size widely vary with location and time. This variation can be attributed to the diversity of sources, gas-to-particle conversion processes, and relatively short atmospheric lifetimes.

1.2 AEROSOLS

Primary aerosols are emitted directly in the air from natural and anthropogenic sources. Secondary aerosols are the result of the gas-to-particle conversion reactions occurring in the atmosphere. Natural aerosol sources include biomass burning, plant process emissions, and volcano debris (Seinfeld and Pandis, 1998). Anthropogenic sources include fuel combustion, industrial processes, roadway dust, wind erosion of cropland, construction debris, and transportation sources (Seinfeld and Pandis, 1998).

Aerosol physical and chemical properties vary regionally. Urban areas are generally dominated by anthropogenic sources, which tend to be densely concentrated around the emission source and largely diluted apart from the source (Seinfeld and Pandis, 1998). Rural and remote regions typically consist of aerosols from natural (e.g., dust, biogenic) sources (Seinfeld and Pandis, 1998). Some rural areas also have some influence from anthropogenic activity (Seinfeld and Pandis 1998), which is often termed as "long range transport" (Seinfeld and Pandis, 1998). The average rural and urban aerosol's fine particle composition is dominated by sulfate and organic carbon (Heintzenberg 1989). Marine aerosols typically derive from sea spray and gas-to-particle conversion reactions. The most common is that of conversion of gaseous dimethlysulfide (DMS), a byproduct of oceanic phytoplankton emissions, to sulfur dioxide (SO_2) and eventually, sulfuric acid (H_2SO_4). The latter either nucleates to form new particles, or condenses rapidly on preexisting particles (Seinfeld and Pandis, 1998). Eventually particles grow to large enough sizes to act as efficient cloud condensation nuclei (CCN).

Once released into the atmosphere, a particle's size and composition can continuously evolve over its average lifetime of a week (Seinfeld and Pandis, 1998). The transformation mechanisms include evaporation, coagulation with other particles, chemical reaction, or activation in the presence of water (Seinfeld and Pandis 1998)..Aerosols are removed from the atmosphere by two different mechanisms: dry and wet deposition. Dry deposition is defined as the transport of particle species from the atmosphere onto surfaces in the absence of

precipitation. Wet deposition includes the uptake of particles by clouds and precipitation with an ultimate surface destination (Seinfeld and Pandis 1998; Haywood and Boucher 2000).

1.3 AEROSOLS AND CLIMATE

Current scientific consensus is that aerosols have an overall cooling effect on the climate (Wigley 1991; Charlson, Schwartz et al. 1992; Penner, Dickinson et al. 1992). Figure 1 shows a report from the International Panel on Climate Change (Houghton, Ding et al. 2001) of annual mean radiative forcings since pre-industrial time that have resulted from different components in the atmosphere. The annual mean radiative forcing best estimate is denoted by the rectangle, and the accompanying bar represents the uncertainty range. The figure illustrates that the aerosol indirect effect can possibly counteract the warming effect of greenhouse gases, but the magnitude of cooling is very uncertain. The vast difference in atmospheric lifetimes of orders of weeks for aerosols and decades for greenhouse gases is also a factor that contributes to this uncertainty (Hobbs 1993).

Aerosols can affect the climate primarily in two ways. First, aerosols intercept solar and terrestrial radiation. Aerosol scattering can be in the form of reflection, refraction, or diffraction of a radiation beam. This is known as the aerosol “direct” effect (Haywood and Boucher 2000; Houghton, Ding et al. 2001).

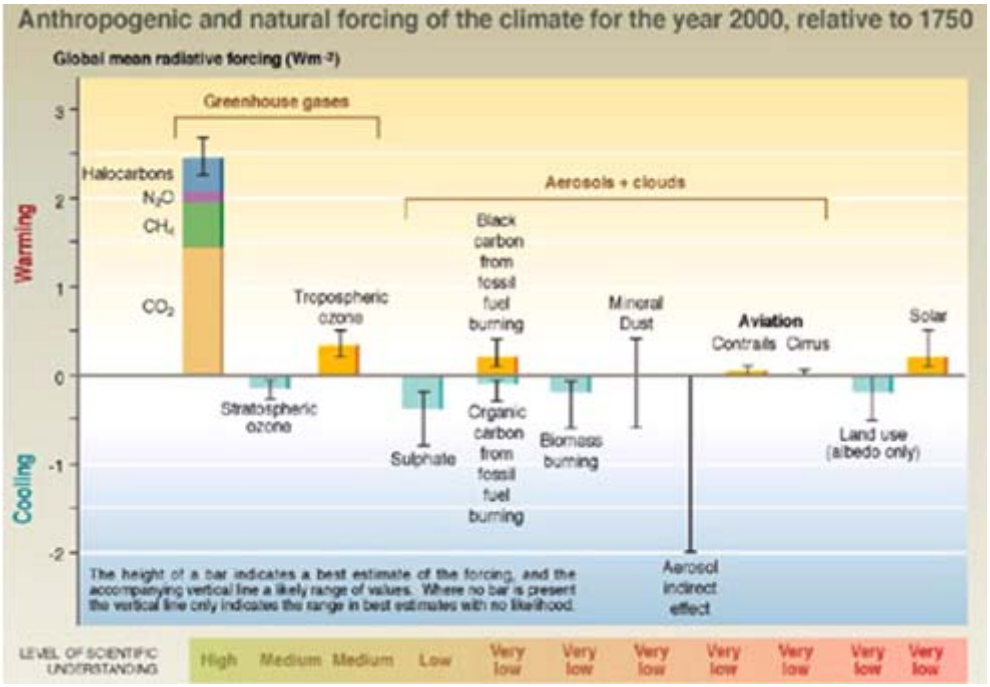

Figure 1: Anthropogenic and natural forcing of the climate for the year 2000, relative to 1750

The direct aerosol effect can either lead to a cooling or warming effect. This is determined by the size, vertical location (Haywood and Boucher 2000), and composition of the intercepting aerosol, the solar zenith angle (Nemesure, Wagener et al. 1995; Pilinis, Pandis et al. 1995; Boucher, Schwartz et al. 1998), the relative humidity (Seinfeld and Pandis 1998; Haywood and Boucher 2000), and the underlying surface reflectance (Haywood and Shine 1995). Aerosol scattering can result in more radiation being reflected back to space, increasing the planetary albedo. Absorbing aerosol, such as mineral dust and soot, can behave similar to greenhouse gases and lead to atmospheric warming (Seinfeld and Pandis 1998; Jacob 1999). Particles efficiently scatter radiation that has a

wavelength comparable to the particle diameter. The maximum intensity of solar radiation occurs at a wavelength of approximately 0.5 μm. Therefore, aerosols in the "accumulation mode", sizes 0.01 μm to 2.5 μm, are typically efficient scatterers in the atmosphere.

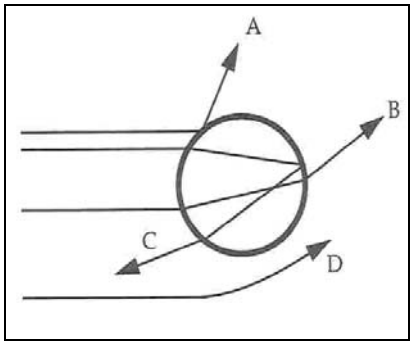

Figure 2: Scattering of a radiation beam. Processes of reflection (A), refraction (B), internal reflection (C), and diffraction (D[AN2])

Secondly, aerosols indirectly affect climate through their interaction with clouds. Clouds are a crucial component in the radiation balance of the earth due to their ability to intercept short-wave solar and infrared terrestrial radiation. Low-level clouds have an overall cooling effect by intercepting and reflecting solar radiation back to space (Baker 1997; Jacob 1999; Houghton, Ding et al. 2001). High-level clouds, such as cirrus, tend to have an overall warming effect because they are transparent to solar short-wave radiation and can prevent terrestrial radiation from returning to space by absorbing it and re-emitting it back to Earth (Hobbs 1993; Baran 2004).

1.4 AEROSOLS AND WARM-LIQUID CLOUDS

Clouds are typically formed when a parcel of air rises and cools until it becomes supersaturated with respect to water (for a liquid-phase, or "warm" cloud) or ice (for an ice-phase, or "cold" cloud). However, a supersaturation of several hundred percent must be present for cloud droplets to form via homogenous nucleation. This cannot happen in the atmosphere because there are plenty of pre-existing particles that serve as heterogeneous nuclei and form droplets at much lower supersaturations, typically fractions of a percent. Cloud condensation nuclei (CCN) are those aerosols that can nucleate cloud droplets at water vapor supersaturations seen in ambient clouds, which range between 0.01 and 2% (Seinfeld and Pandis, 1998). The composition and size of the CCN determine what supersaturation is needed for activation to cloud droplets (Seinfeld and Pandis 1998). When this "critical" supersaturation is reached, the particles activate continue to grow and form cloud droplets. Kohler in the early 20th century used thermodynamic arguments to express the water vapor supersaturation, $S = \frac{P^w}{P^{sat}} - 1$, in equilibrium with a deliquesced CCN of wet diameter D_p, containing n_s moles of dissolved solute,

$$S = \frac{4M_w\sigma_w}{RT\rho_w D_p} - \frac{6n_s M_w}{\pi\rho_w D_p^3} \quad (1)$$

where P^w is the ambient water vapor pressre, P^{sat} is the water saturation vapor pressure, M_w is the molar mass of water, σ_w is the air-water surface tension, R is the universal gas constant, T is the temperature, ρ_w is the water density. The first part of equation (1) accounts for the Kelvin effect, which states that the vapor pressure over a flat surface of a substance is higher than the vapor pressure over a curved surface of the same substance. The second part of equation accounts for the solute effect, which is related to Raoult's law, which states that the vapor pressure over a solution is decreased as more solute is added to the pure solvent. Equation 1 has a maximum equilibrium supersaturation, termed the "critical supersaturation" beyond which the droplet is in unstable equilibrium with water vapor. In practical terms, any CCN that has been exposed to a supersaturation larger than its critical supersaturation for long enough time to exceed the maximum of Equation (1), experiences unstable and unconstrained growth. When this happens, the CCN is said to have become "activated" and is a "cloud droplet".

Anthropogenic emissions tend to increase the concentrations of aerosols, and hence, the concentration of CCN. Thus, when cloud form in polluted airmasses, they tend to contain higher concentrations of cloud droplets compared to cleaner conditions (Seinfeld and Pandis, 1998). This generally leads to clouds with smaller droplet size; as a result, the cloud's reflectivity is increased, because there is more surface area to interact with incoming solar radiation. This is known as the "aerosol first indirect radiative effect".

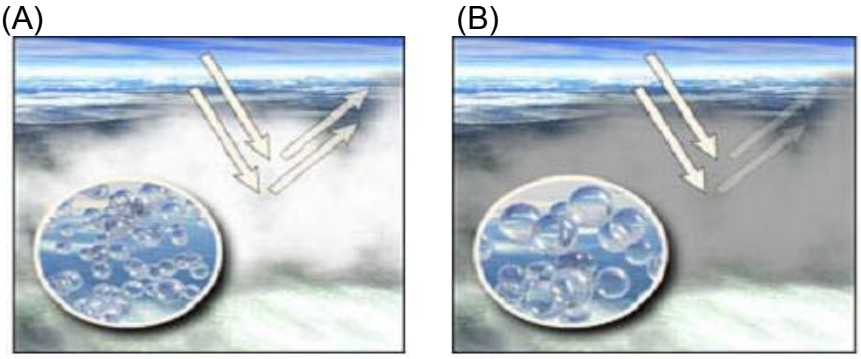

Figure 3A,B: The First indirect effect of aerosols on climate (Ranson 2004)

Figure 3A represents a cloud formed in a polluted air mass that provides a large number of nucleation sites for cloud formation. The large number of cloud droplets leads to a greater reflection of the solar radiation back to space creating a brighter cloud. Figure 3B shows a cloud that has a lower amount of cloud droplets resulting in a less reflective cloud. An increase in aerosol cloud concentrations also lead to rain suppression and is known as the "second indirect effect" (Albrecht 1989). Several other studies have been conducted to understand and quantify the indirect effects (Coakley et al. 1987; Radke et al. 1989; Leaitch et al. 1992; Hegg et al. 1993; Martin et al. 1994; Novakov et al. 1994)[AN6]. Despite the numerous studies published in the literature, of the uncertainty associated with quantifying the second indirect effect is substantially larger than the first, to the point that the last IPCC does not even provide a quantitative estimate.

1.5 AEROSOLS AND MIXED-PHASE AND ICE CLOUDS

Aerosols can also behave as ice nuclei. Therefore, the aerosol indirect effect may also play a role in the formation, microphysical properties, and optical properties of ice and mixed-phase and ice clouds. Lohmann and Feichter (2004) report that an increase of ice water content can lead to the same indirect effect seen in liquid water clouds and to a infrared radiative effect. However, the magnitude of indirect effect is highly uncertain, even more than that associated with the first and second indirect effects (Houghton et al. 2001; Lohmann and Feichter 2004).

Cirrus are high altitude clouds that have a silken appearance, consist of ice crystals, and cover between 20% and 50% of the globe (Dowling and Radke 1990; Baran 2004).The cirrus cloud thickness is typically 1.5 km, and the average horizontal span is 20 to 30 km (Dowling and Radke 1990). The vast presence of these clouds makes them an essential component in the global radiation budget (IPCC, 2001).

Cirrus cloud formation begins with the nucleation of ice crystals. Ice crystals form and grow by several different mechanisms, which are sensitive to temperature, humidity, and atmospheric composition (Baker 1997; Heymsfield, Bansemer et al. 2004). Homogenous nucleation most often occurs at very low temperatures, typically below -40˚C, and at very high supersaturations with respect to ice. This process is called freezing mode. The freezing mode is described as a supercooled droplet transforming directly into the ice phase.

Freezing involving a nucleation site known as Ice Nuclei (IN) is heterogeneous freezing. Aerosols that are insoluble, such as dust and combustion particles, and have similar molecular bonding and structure as ice are the typical IN (Seinfeld and Pandis 1998; Houghton et al. 2001). Heterogeneous freezing has been observed to occur at temperatures as high as 0°C and at lower supersaturations than homogenous freezing. The heterogeneous freezing modes are illustrated in figure 4.

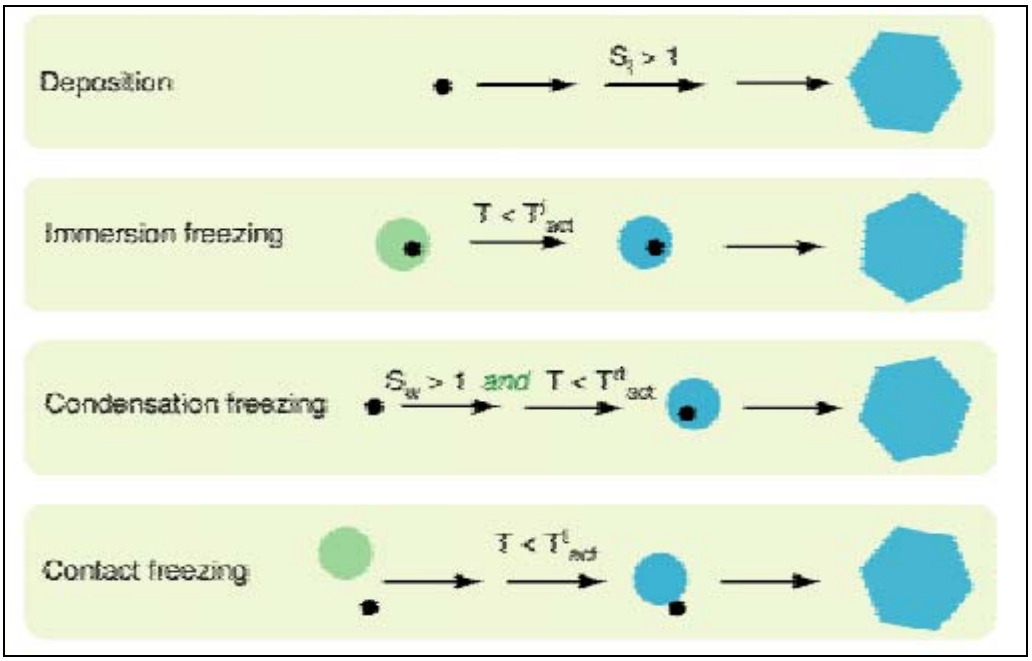

Figure 4: Schematic depiction of nucleation modes of ice in the atmosphere (Vali 1999)

Deposition entails the adsorption of water vapor onto the surface of the Ice Nuclei (IN) surface resulting in a conversion to ice. Immersion freezing is the freezing of a supercooled drop with an immersed IN. Condensation freezing occurs when water vapor condenses onto an IN and subsequently freezes. Contact freezing is the collision of a supercooled droplet with an IN.

It has been shown that at certain temperatures and relative humidity values the ice particle freezing mode affects the ice particle growth rate and eventually the microphysical properties of the cloud (Khvorostyanov and Sassen 1998; Bailey and Hallett 2004). The ice crystals grow by collision with supercooled droplets and vapor diffusion. Therefore, the rate of growth mechanisms can be controlled by the availability of water vapor or the concentration of supercooled droplets.

The characteristics of the ice particles within cirrus clouds can strongly impact the cloud's optical properties (Matrosov, Heymsfield et al. 1995). Typically, optical properties are parameterized in terms of the cloud's ice water content (IWC), and ice crystal morphology, or "habit", and ice particle size distribution (Baran 2004). The most common ice habits are columns, bullets, bullet rosettes, hexagonal plates (Fig. 5), and aggregates of the former (Dowling and Radke 1990; Baran 2004). Studies have shown that the crystal habit is dependent on temperature, humidity, and ice nucleation and growth mechanisms (Heymsfield and McFarquhar 1996; Baker 1997; Heymsfield and Miloshevich 2003; Bailey and Hallett 2004). The variety of ice crystal formation mechanisms, shapes, size distributions, and concentrations, coupled with the limited data

available contribute to the difficulty in characterizing the clouds' properties and microphysical processes.

Effective radius, extinction, and optical depth are all radiative properties that are dependent on the particle size distribution and ice water content. The effective radius is defined as the ratio of the second to third moment of the particle size distribution. The measure of the amount of light that is allowed to pass through a specified medium is the optical depth. Ebert and Curry (1992) observed that the extinction of the optical depth per unit cloud thickness can be determined by the ratio of the IWC to the effective radius or total particle cross-sectional area. The role of small ice crystals has been the focus of some recent studies. McFarquhar and Heymsfield (1997) observed that 56% of the total extinction was due to the contribution from crystals smaller than 90 μm. It was also observed that the reflectivity values simulated by the MODIS airborne simulator were very sensitive to the numbers and shapes of small crystals (McFarquhar, Heymsfield et al. 1999). Small particles have also been observed to sometimes dominate cirrus clouds' solar extinction and long-wave emission during in-situ observations and calculations by Arnott, Dong et al (1994).

ICE CRYSTAL HABIT	CHARACTERISTIC IMAGE
Columns **(Heymsfield and Miloshevich 2003)**	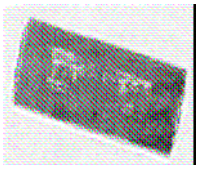
Bullets **(Villa, Cruz-Pol et al. 2002)**	
Bullet Rosette **(Heymsfield and Miloshevich 2003)**	
Plates **(Heymsfield and Miloshevich 2003)**	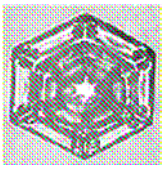

Figure 5: Most common ice particle habits in cirrus clouds

1.6 THE NEED FOR IN-SITU DATA

The improved understanding of cirrus cloud microphysical properties, such as ice water content, cloud particle phase, ice particle habit, and particle size distribution, is contingent on acquiring and analyzing data from cirrus clouds. In-situ data is needed to construct and validate parameterizations of radiative properties of mixed-phase and ice clouds. However, cirrus' cloud data acquisition can be challenging, because of the extreme environments usually associated with cirrus clouds. Several research aircraft missions have been conducted to gain more information about ice and mixed-phase clouds. Some of these missions include: CEPEX (Heymsfield, McFarquhar et al. 1998; McFarquhar, Heymsfield et al. 1999), SHEBA (Wyser and Jones 2005; Zuidema, Baker et al. 2005), FIRE-ACE (Lawson, Baker et al. 2001; Marchand, Ackerman et al. 2001), CRYSTAL-FACE (McGill, Li et al. 2004; Mitrescu, Haynes et al. 2005). However, research aircraft missions are expensive and only short-term which does not allow enough data to be collected to represent long-range properties. Collecting data from cirrus clouds can also be hazardous because of icing concerns.

Small robotic aircraft know as Unmanned Aerial Vehicles (UAVs) have recently been used in several missions, which open opportunities for cost-effective long-range environmental studies in remote and harsh weather conditions (Holland, Curry et al. 2001). These aircraft have the ability to carry instruments that can gather in-situ data about various microphysical properties of

clouds such as cloud particle phase, particle size distribution, ice crystal habit, and liquid and ice water contents.

The mini Video Ice Particle Sampler (mini-VIPS) is an instrument that is being positioned on UAVs to take images of ice particles in cirrus clouds. It has the ability to accurately take images and measure ice particles at a low detection limit of 5 μm, which is lower than the detection limit of most other instruments. The characteristic differences of these small crystals, such as size, shape, and number distributions, can have a significant effect on the radiative properties of cirrus clouds. Therefore, it is vital to the improvement of current climate models to understand, quantify, and include these effects by using UAV in-situ data.

1.7 GOALS OF THIS THESIS

The VIPS performance has been investigated in a small number of studies (Heymsfield and McFarquhar 1996; McFarquhar and Heymsfield 1996; McFarquhar, Heymsfield et al. 1999). The miniaturized version, mini-VIPS, has just recently been utilized in UAV missions, but has not undergone the same type of analysis and validation. The purposes of this study are as follows:

(1) To validate the mini-VIPS performance by comparing the mini-VIPS data retrieved during an Artic UAV mission on March 2004 in Barrow, Alaska with data acquired from remote sensing instruments at the Barrow, Alaska ARM/CART site

(2) To analyze the mini-VIPS data to survey the properties of high-latitude cirrus clouds

CHAPTER 2

ARCTIC CLOUDS

The arctic is defined as the region above the Arctic Circle, which is located at 66° 32' N Latitude. Parts of Alaska, Canada, Denmark, Finland, Greenland, Iceland, Norway, Russia, and Sweden are some land areas located in the Arctic region. The arctic environment is extreme and is characterized by limited sunlight, extreme temperatures, short growing season, dry atmosphere, and continual presence of land and sea ice and snow. The Arctic regions predicted to be very sensitive to global climate change (Meehl and Washington 1990; Houghton, Gallimore et al. 1991; Houghton, Ding et al. 2001). The high coverage of snow greatly contributes to the climate sensitivity. The snow's high reflectivity, high infrared emissitivity, and high insulating property are the sources of numerous snow climatic feedbacks. The properties lower the surface net radiation balance, produce lower-tropospheric temperature inversions, and impede the transfer of heat between the atmosphere, land, and sea ice (Pryzybylak 2003).

Arctic clouds play a significant role in the region's climate (Curry et al. 1996; Garrett et al. 2001; King et al. 2004; Shupe and Intrieri 2004). There have been several observations made about Arctic clouds. Curry et al (1996) reported that majority of arctic clouds are low-lying, optically thin clouds. Isaac and Stuart

(1996) studied clouds in the Mackenzie Valley-Beaufort sea area and observed stratocumulus as the dominant cloud type. This is in agreement of Warren et al (1985) observation of dominant stratiform clouds over Alaska. Low lying, thin stratus clouds are reported by Lawson et al (2001)[AN7] as the most frequently observed arctic clouds during SHEBA

Cloud coverage and properties change seasonally in the arctic. November to April is designated as the winter period and is characterized by mean cloud coverage between 40% and 60%. The summer period from May to October has much greater cloud coverage of 80% -90%, which is mainly contributed to an increase in low-level clouds. Abrupt cloud coverage increase and decrease is observed in the spring and autumn transition periods respectively (Pryzybylak 2003).

The thermodynamic phase of Arctic clouds is very important for understanding their microphysical and optical properties. Arctic clouds can be composed of both liquid droplets and ice crystals. Ice crystals are dominant in winter arctic clouds (Wilson et al. 1993); however, liquid water clouds are still prevalent during this time frame (Curry et al. 1988). Spring and autumn time frames are characterized by mixed-phase clouds or clouds with a fraction of ice crystals and liquid water droplets (Gultepe et al. 2000). It can be inferred that mixed-phase clouds have the potential to represent up to 66% of arctic clouds from Shupe et al's (2001) observation that uniform phase (i.e. all liquid or all water) radar retrieval [AN8]methods were only valid 34% of the time. McFarquhar and Cober (2004) observed phases, shapes, and sizes of cloud particles from in-

situ measurements taken during the FIRE-ACE campaign, and concluded that mixed-phase clouds are frequent in the arctic region.

The types and thermodynamic and microphysical properties (i.e. phase, size, and shape) of arctic clouds are important factors in how Arctic clouds affect the climate. Arctic clouds impact the climate in several ways by its interactions with the onset and rate of annual snowmelt (Curry, Rossow et al. 1996; Zhang, Stamnes et al. 1996) and by affecting atmospheric heat and moisture profiles (Gultepe, Isaac et al. 2000; Shupe and Intrieri 2004). The feedback between cloud radiation and snow/ice albedo are also interrelated in the Arctic (Curry, Rossow et al. 1996) and is affected by a change in the onset of ice melting. Gultepe et al (2000) reported that latent and sensible fluxes were increased as a result of melting layers and their production of wind shear and strong temperature gradients. A change in the heat and moisture profiles plays a role in the formation of clouds and the hydrological cycle (Gultepe et al. 2003).

The Arctic region is associated with a number of uncertainties in cloud properties and cloud-climate interactions. Primary uncertainties in the arctic region include cloud particle phase (Curry et al. 1996; Turner 2005), arctic cloud ice water contents (IWC), effective size, and particle shape (Ghan et al. 1997; Gultepe et al. 2003), the role of aerosols on the phase and phase transition of arctic clouds (Curry et al. 1996), the response of climate in respect to the greenhouse warming betweens due to arctic clouds (Curry et al. 1996), the response of the arctic surface radiative properties due to changes in snow characteristics (Curry, et al. 1996), and the relationship between the cloud-

radiative and ice-albedo feedback mechanisms (Curry et al. 1996). It is imperative to learn about the microphysical properties of arctic clouds. Lawson et al (2001) state that the prediction of trends of arctic boundary layer cloud microphysical properties is difficult due to the lack of measurements. It was concluded by Gultepe et al (2000) that better in-situ methods with current technology are needed to be able to accurately represent arctic clouds' IWC values. The ice water content in conjunction with the cloud particle size distribution and habit distribution are all factors that contribute to arctic cloud radiative properties. In summary, the arctic is very sensitive to climate because of its extreme conditions. However, instrumentation and campaigns suitable for the Arctic environment are needed to better understand this region.

CHAPTER 3

DESCRIPTION OF REMOTE SENSING AND IN-SITU INSTRUMENTATION

3.1 IN-SITU INSTRUMENTATION

The role of small ice crystals in relation to cirrus cloud radiative properties is still largely unknown (Takano and Liou 1989; Kinne, Ackerman et al. 1992; McFarquhar and Heymsfield 1996; McFarquhar et al. 1999), primarily due to the limitations of in-situ instrumentation. Several instruments including Particulate Volume Monitor (PVM) (Gerber, Arends et al. 1994), Counterflow Virtual Impactor (CVI) (Noone, Noone et al. 1993; Strom and Heintzenberg 1994; Twohy, Schanot et al. 1997; Gerber, Twohy et al. 1998; Gayet, Auriol et al. 2002), Forward Scattering Spectral Probe (FSSP) (Fleishauer, Larson et al. 2002; Baumgardner, Chepfer et al. 2005), Two Dimensional Cloud Probe (2D-C), and the Polar Nephelometer have been used to detect ice particles in high level cirrus clouds. These instruments either cannot detect small particles, or rely on an a-priori assumption of particle shape, which usually results in the incorrect estimation of the number and size of small particles. For example, the PVM is limited to a 50 μm diameter that is also sensitive to ice crystal shape (Gerber, Twohy et al. 1998). McFarquhar and Heymsfield (1996) also observed that the 2D-C probe only provided reliable measurements for particles greater than 100 μm at jet speeds at or above 200 m s^{-1}.

The FSSP, CVI, PVM, and 2DC probe are examples of instruments that obtain indirect measurements. The FSSP determines the size of particles by measuring the amount of light the particle scatters in the forward direction (Fleishauer et al. 2002). The CVI operates by evaporating ice crystals that have been inertially separated from the atmosphere and measuring the quantity of resulting water vapor (Gerber et al. 1998; Gayet et al. 2002). This instrument indirectly measures the ice water content (IWC) and estimates the mean volume radius and number of ice crystals per ice volume. The particulate volume monitor (PVM) optically measures the IWC of crystals and provides an estimate of the effective radius and number of ice crystals per unit cloud volume (Gerber et al. 1998). The two-dimensional cloud (2DC) probe attains crystal sizes and shapes by measuring the image of the particle's shadow.

The limitations of the FSSP include its assumption of spherical particles and over estimation of the ice crystal concentration in the presence of large particles (Gardiner et al. 1985; McFarquhar and Heymsfield 1996; Gayet et al. 2002). Gayet et al (1998) hypothesize that the shattering of large particles onto probe inlets for the FSSP, CVI, and polar nephelometer instruments can explain observed over-counting of small particles. The other limitations of the 2DC probe include over-sizing of out-of-focus particles (Lawson et al. 1998; Strapp et al. 2001) and delayed response time that leads to under-sizing and undercoating of smaller particles (Baumgardner and Korolev 1997; Strapp, Albers et al. 2001), particle distortion at high jet speeds, and inaccuracies when the ice concentration is high (Fleishauer, Larson et al. 2002).

3.2 VIDEO ICE PARTICLE SAMPLER (VIPS)

The VIPS, developed by Dr. Andy Heymsfield from the National Center for Atmospheric Research, collects a continuous sample of cloud ice particles on an 8-mm wide “conveyor-belt” film. The film is coated with silicon to cushion impact of the ice crystals. The instrument contains an electro-optical and imaging component for collecting data, and a data acquisition and recording unit. The collection unit’s aperture width can be adjusted thereby corresponding to different flight conditions. Once the sample has been collected, two video microscopes at different magnifications record the image. The data can then be analyzed immediately after the flight to determine size and habit classifications.

The VIPS can detect particles from 5 μm to greater than 150 μm in diameter with an accuracy of ±10 μm. The VIPS provides a direct measurement of ice crystals and is not restricted to spherical particles like the FSSP. It has also been observed that only ice crystals with a diameter larger than 200 μm fracture upon impact (McFarquhar and Heymsfield 1996). The limitations of the VIPS include time consuming and tedious data analysis, image quality variations, and instrument saturation at high Ice Water Contents (IWC) (McFarquhar, Heymsfield et al. 1999). However, the direct measurement and ability to image small particles render the VIPS as a powerful instrument that can significantly improve our understanding of cold cloud microphysical processes, as well as provide us with improved parameterizations of ice cloud microphysics useful for Global Climate Models (GCMs) and remote sensing retrievals.

Figure 6: Photo of mini-VIPS

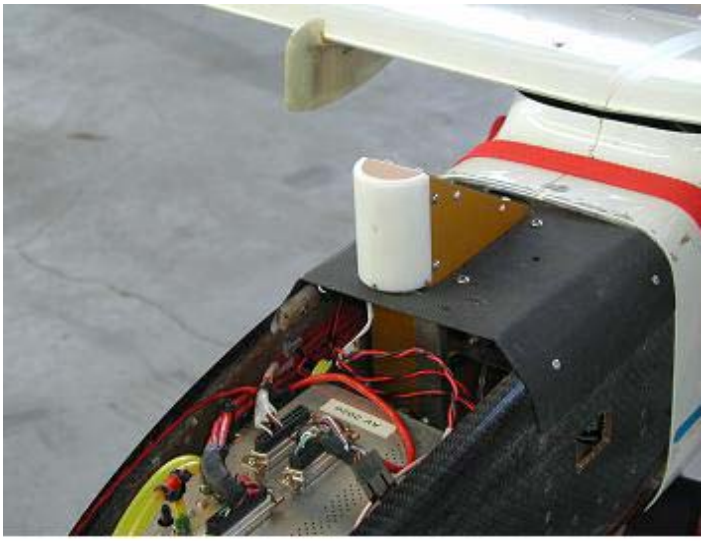

Figure 7: Photograph of mini-VIPS mounted on Aerosonde Aircraft

3.3 MILLIMETER –WAVELENGTH CLOUD RADAR (MMCR)

In response to the need to improve the representation of clouds in climate models, the Department of Energy (DOE) initiated the ARM program (Stokes and Schwartz 1994) The ARM program has 3 CART sites throughout the world. A site exists in Barrow, Alaska, the most northern point of the United States, to aid the study of cirrus cloud properties. Figure 8 shows the map of Barrow, Alaska and the location of the ARM/CART Site. The millimeter-wave cloud radar (MMCR), pictured in figure 9, has been developed for continuous long-term observation of cloud properties at various ARM/CART sites. The MMCR is a vertically pointing radar that operates at a frequency of 35Ghz and 8.6-millimeter wavelength. 35Ghz is an atmospheric window where attenuation due to water vapor and oxygen is minimal. The operation at 8.6 millimeters is a tradeoff between the greatest sensitivity to cloud particles and least attenuation of the radar beam by atmospheric particles (Clothiaux et al. 2001). The short wavelength of the MMCR also allows it to observe greater details the formation and microphysical properties of clouds (Hollars et al. 2004).

The MMCR can provide vertical profiles of cloud macrophysical properties such as cloud boundaries, radar reflectivity, and vertical velocities. Additionally, the MMCR can provide cloud microphysical data in combination with other remote sensing instruments. The microphysical parameters that can be estimated include hydrometeor sizes, concentrations, and ice and liquid water mixing ratios.

The MMCR operates in four different modes by changing the sensitivity level to detect different type of cloud particles. Mode 1 has high sensitivity and vertical resolution and is known as the "boundary layer stratus mode." It is sensitive to weakly reflecting, lower-level, liquid droplet clouds. Mode 2 or "cirrus mode" detects weakly reflecting mid and higher-level ice clouds. Mode 3, "General Mode", and Mode 4, "Robust Mode" are the least sensitive modes. They can respectively detect cloud particles and reflectivity values at all altitudes (Clothiaux, Miller et al. 2001).

The MMCR has several advantages as a remote sensing cloud-detecting instrument[AN9]. Moran et al (1998) discusses the significant sensitivity of MMCR to small cloud particles, and, with significant spatial resolution. Hollars et al (2001) reports that the MMCR, in most cases, provides accurate cloud retrievals at cloud-top height. Unlike its predecessor, the NOAA/K radar, the MMCR produces reliable results for long-term, unattended observations (Moran et al. 1998). The compactness of the MMCR facility is highly desirable; powerful transmitters or huge antennas are not required for its operation (Moran et al. 1998).

Conversely, there are also some disadvantages associated with the MMCR. During sampling of optically thick clouds and periods of heavy precipitation severe attenuation of the radar beam is experienced (Moran, Martner et al. 1998; Clothiaux, Miller et al. 2001). MMCR also have more limited range cover when compared to precipitation radars (Moran, Martner et al. 1998).

Figure 8: Map of ARM site and ARM duplex locations in Barrow, Alaska


Figure 9: Photograph of the Millimeter Wavelength Cloud Radar (MMCR)

3.4 IN-SITU VERSUS GROUND-BASED MEASUREMENT

Both remote sensing techniques and in-situ measurements are important for a greater understanding of the microphysical properties of clouds. As stated by McFarquar and Heymsfield (1996), “Remote sensing can be used to examine larger areas of cirrus with better time resolution, but in-situ observations are needed to determine the numbers, shapes, and sizes of crystals.” Previous studies (Wang and Sassen 2002) have used the intercomparison of in-situ and ground-based measurements to validate the ground-based retrieval methods. Since these methods have already been explored, they can now be used to validate the mini-VIPS in-situ data.

CHAPTER 4

OBSERVATIONS AND ANALYSIS METHODOLOGY

4.1 FLIGHT MISSION DESCRIPTION

The Aerosonde UAVs were deployed in an Artic Operations program in 2004, spearheaded by the University of Colorado at Boulder and funded by the National Science Foundation (give name of mission, if available and website URL). The clouds were sampled during a cirrus cloud mission on 28 March 2004 UTC and 29 March 2004 UTC in the vicinity of Barrow, Alaska. The Aerosonde, operated and designed by Aerosonde Ltd and Aerosonde North America (www.aerosonde.com), is a UAV that has been designed for a wide range of operations. The temperature, pressure, and relative humidity are all measured by the Vaisala RSS901 sensors mounted on the aircraft, while the winds are calculated from GPS data (Curry et al. 2004). Instruments are able to be mounted in a clean exhaust-free environment as a result of the Aerosonde's "pusher" configuration (Holland et al. 2001). The Aerosonde's operation is commanded and controlled remotely. It can be operated with a combined instrument and fuel payload of up to 7 kg. Because of this, there is always a tradeoff between payload and maximum flight range. The mini-VIPS is mounted on the Aerosonde UAV to acquire data.

The Aerosonde aircraft, AC 107, was launched for a period of measurement of approximately five hours and 41 minutes lasting from 28 March 2004 20:24:00 UTC until 29 March 2004 2:26:53 UTC. There were three components of this flight. The flight began with the aircraft flying above the runway for several circuits. Next, a step profiling is done starting at 1500 m. Lastly, the aircraft descended at 200m intervals performing 5-10 minute 1 km box patterns. The flight path, shown in figure 10, and the latitude and longitude plots (Figures 11 and 12) show how the Aerosonde is flown between the latitudes of 71.34°N and 71.42°N and longitudes of 156.44°W and 156.66°W.

In addition to the mini-VIPS, the aircraft also carried probes to record ambient temperature, pressure, and relative humidity over liquid water. The relative humidity over ice was calculated from the observed data. Figure 14 displays the atmospheric pressure recorded during the flight. The atmospheric pressure stays in the range from approximately 850mb to 1050mb. The ambient temperature (Figure 15) is fairly constant, ranging between -30°C and -33°C. The higher temperatures seen at the earlier times represent the near surface temperature, consistent with the aircraft's altimeter reading close to 0. The relative humidity (figure 16) is varies significantly. The relative humidity with respect to ice is always larger than the relative humidity with respect to water. Throughout the flight, the relative humidity with respect to ice is mostly in between 60%-100% while the relative humidity with respect to water is mostly in between 45% -75%. The time period after 21:10:00 UTC where the sample volume is saturated with respect to ice indicates a likely location for the formation

of ice/mixed-phase clouds. Greater details of the Aerosonde aircraft and the diary of this mission can be accessed at www.aerosonde.com.

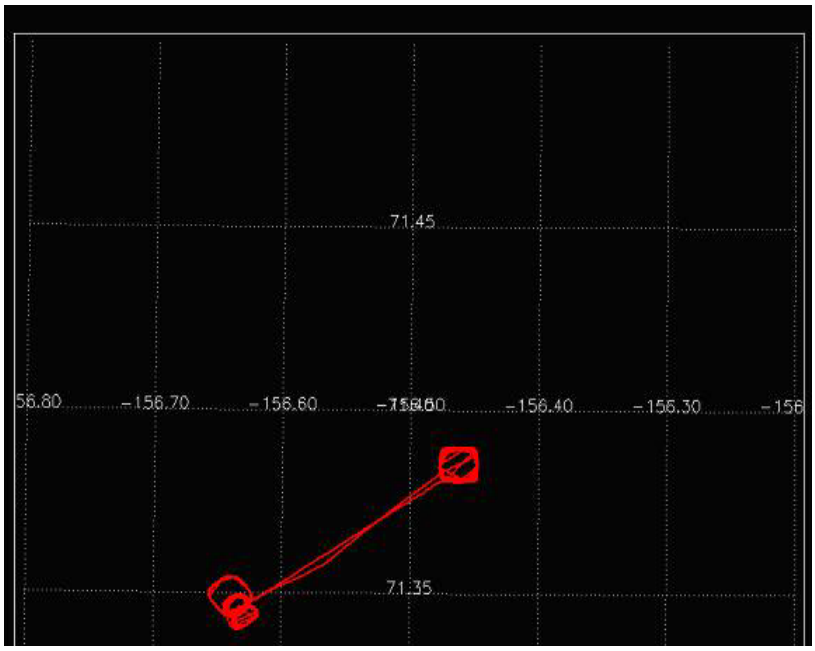

Figure 10: Flight path of the Aerosonde UAV in Barrow, Alaska on March 28-29, 2004 UTC. The mini-VIPS was mounted on the Aerosonde

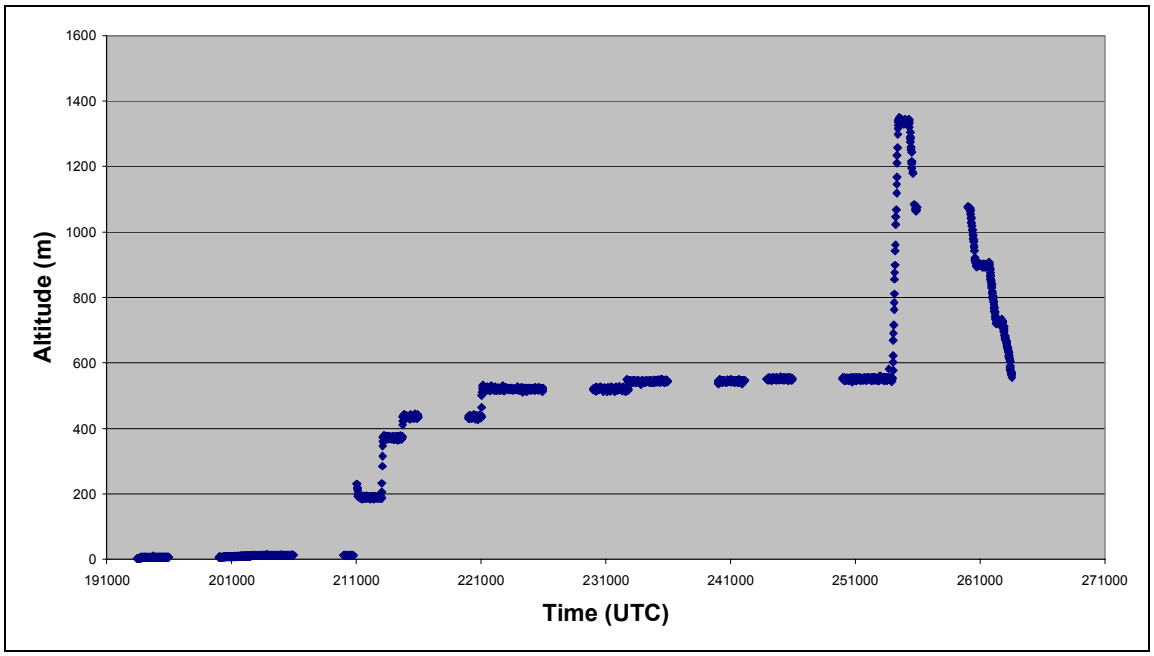

Figure 11: Recorded Altitude during March 28-29, 2004 UTC flight

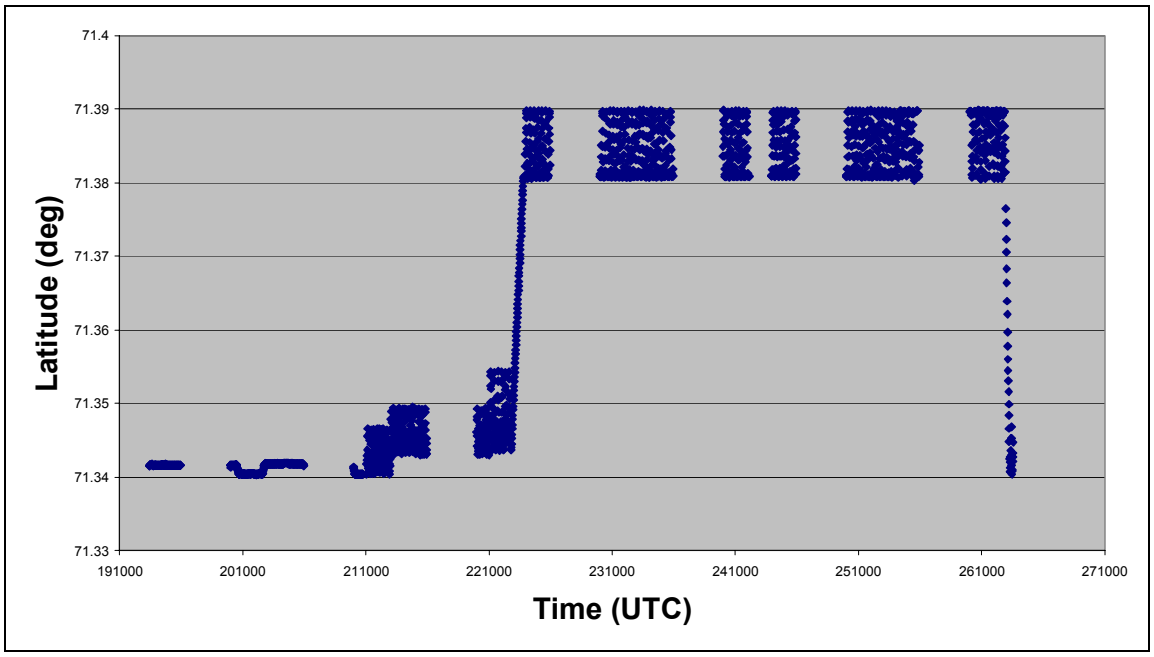

Figure 12: Recorded Latitude for March 28-29, 2004 UTC flight

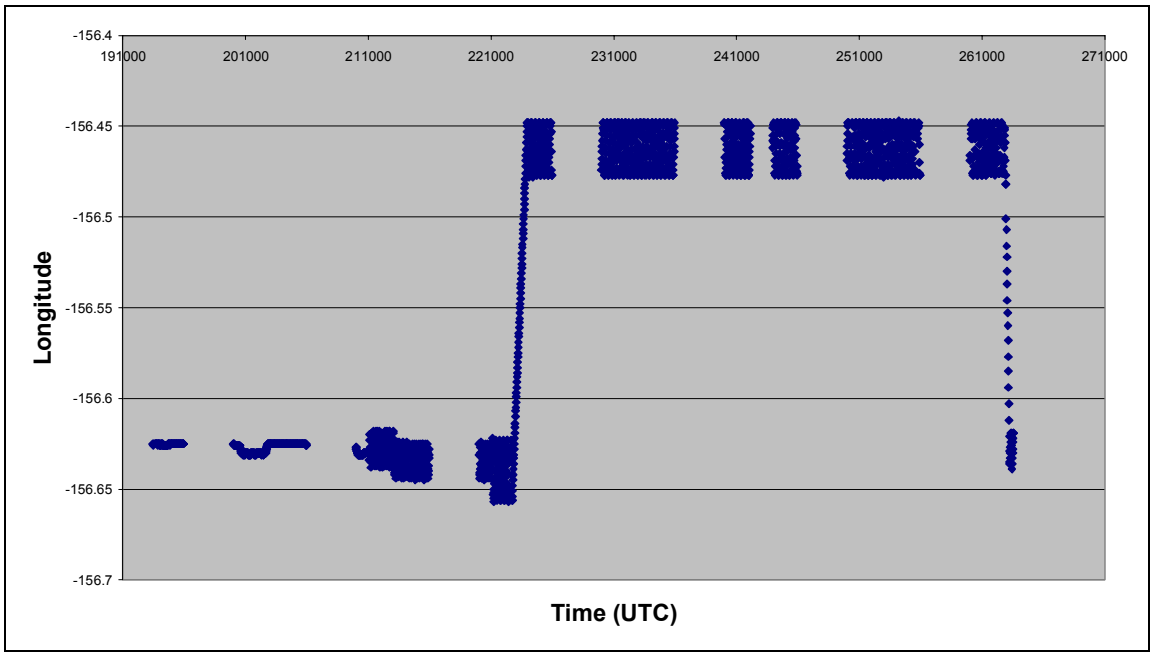

Figure 13: Recorded longitude values for March 28-29, 2004 UTC flight

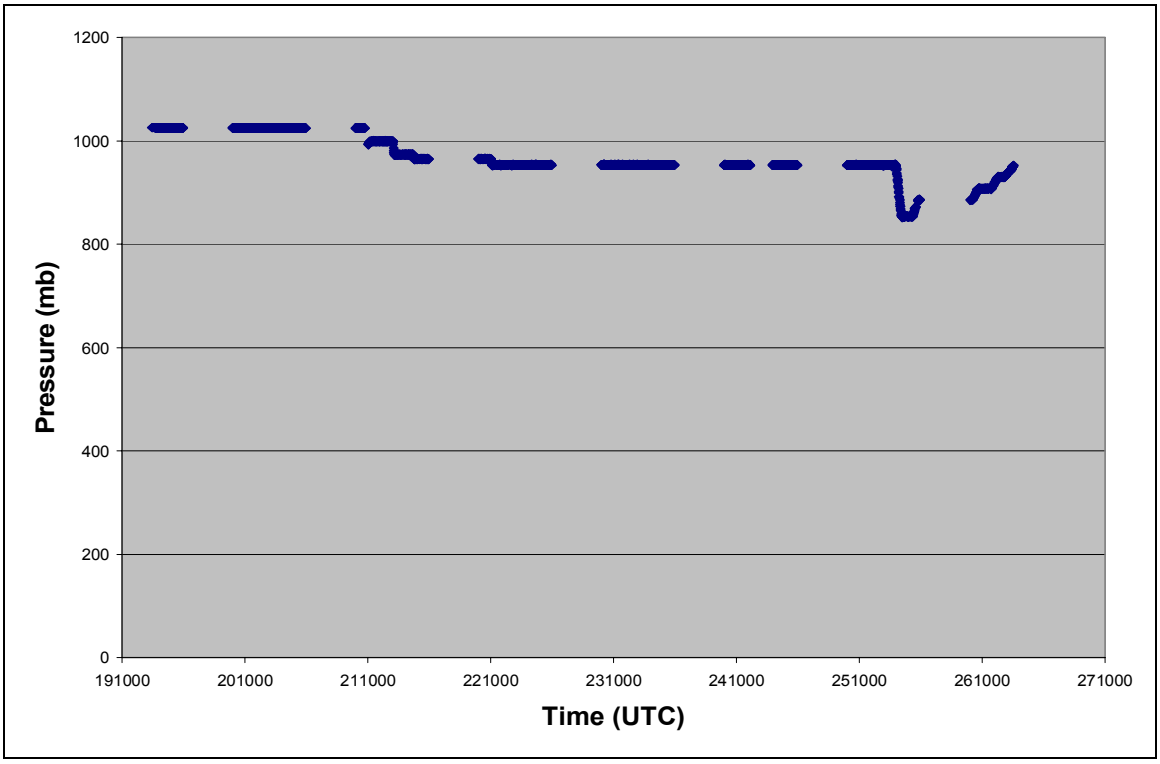

Figure 14: Recorded pressure values for March 28-29, 2004 UTC flight

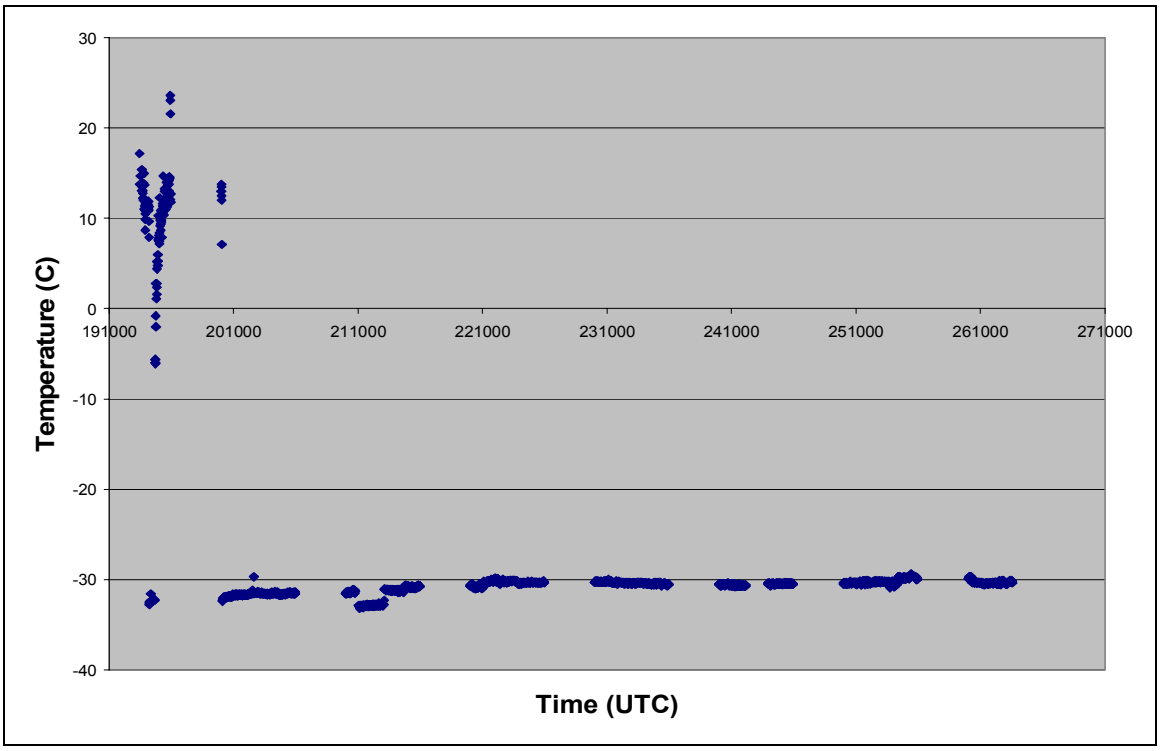

Figure 15: Ambient Temperature Recorded on March 28-29, 2004 UTC flight

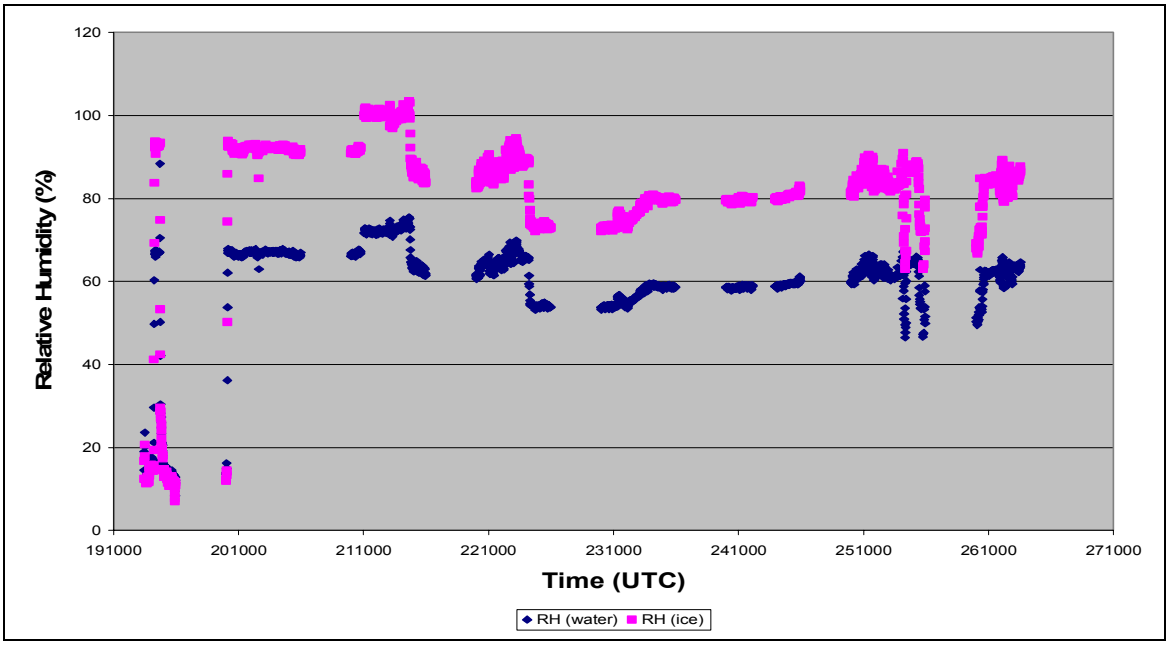

Figure 16: Relative Humidity with respect to water and ice during March 28-29, 2004 UTC flight

4.2 MINI-VIPS PROCESSING

The mini-VIPS instrument records the collected sample of ice particles on a digital videotape. Frame capturing software is then used to convert the video footage to still frame shots. Only the time frames where ice particles were observed were considered for capturing. Approximately 2000 frames were captured from the Barrow mission. The images are then further analyzed with an IDL program. This code processes each image and determines the time, concentration (#/L), extinction (1/km), total surface area (cm^2/cm^3), mass (g/m^3), number distribution, and the area ratio of the ice crystals found in the images. The sample volume in liters per second is calculated per pixel, and then multiplied by the number of pixels.

$$t_e = \frac{w_s}{s_f} \tag{2}$$

Where t_e (s) $_{is}$ the time the film is exposed to the air, w_s (mm) is the width of the sampling slit, and s_f (mm s^{-1}) is the speed of the film.

$$v_s = \frac{t_e * n_p * \sigma_p{}^2 * s_a}{1000} \tag{3}$$

Where v_s (L s^{-1}) $_{is}$ the sample volume, n_p is the number of pixels ($count^{-1}$), σ_p is the pixel size (cm), and sa is the speed of the air (cm s^{-1})

The concentration is defined as the number of ice particles found in the sample volume. The number of particles in the sample volume is determined by using a function that counts the number of unique regions within the image. The concentration is then defined as the unique regions divided by the sample volume.

$$C = \frac{n_r}{v_s} \tag{4}$$

Where C is the particle concentration per second (L^{-1} s^{-1}) and n_r is the number of regions on the captured frame.

The extinction is defined as the scattering and absorption of an object that decreases the radiation received by satellite sensors (Glickman 2000)[AN10]. The extinction, ε, is estimated as,

$$\varepsilon = \frac{A_T * 2000}{10} \tag{6}$$

where A_T (cm^2 l^{-1}) is the total area of all particles, $A_T = \frac{\sum A_p}{V_s}$, and A_p (cm^2 l^{-1}) is the area of the individual particles.

The total area , A_T, represents the combined cross-sectional area of all of the ice particles combined. The particles in the frame that have an extinction value of less than 2.0 get used for analysis. Further analysis includes the calculation of the maximum length and area ratio of each particle. The area ratio as defined by Heymsfield and Miloshevich (2003) as the ratio of a particle's projected cross-sectional area to the area of a circle having the particle's maximum diameter. This value can provide insight about a particle's shape. The surface area is then defined as a function of the area ratio.

$$A_s = A_T * 5.6 * A_R^{-0.65} \tag{7}$$

Where A_s is the surface area and A_R is the area ratio.

The empirical relationship from the Cirrus Regional Study of Tropical Anvils Cirrus Layers-Florida Area Cirrus Experiment (CRYSTAL-FACE) citation data is then used to calculate the ice water content (IWC)

$$IWC = 0.0061 * \left(\frac{I_p}{1000} \right)^{2.05} \tag{8}$$

Creating a histogram from 0 to 500 μm divided in 50 10-μm size bins then produces the particle size distribution. Their maximum length characterizes the particles. Being divided by 10 μm, the size of each size bin, normalizes each bin concentration. The same 50 size bins are used to produce the area ratio

distribution. Again, the particles are classified by their maximum length. Next, the average of all the area ratios of each particle is assigned to the corresponding bin.

4.3 INTERCOMPARSION

Several studies have compared in-situ reflectivity and ground-based reflectivity to verify ground based retrieval methods or to verify in-situ data (Heymsfield 1977; Matrosov, Heymsfield et al. 1995; Matrosov, Heymsfield et al. 1998; Wang and Sassen 2002). One of the main challenges in this procedure is attempting to compare measurements from the same sample volume. Therefore, it is important to ensure that the In-situ measurements are in close vicinity to the MMCR location. The ARM MMCR is located at a latitude and longitude of 71.323 (1.245 rad) and –156.609 (-2.733 rad) respectively. The aircraft was flying in the latitude range from 71.34° (1.2451 rad) to 71.42° (1.2465 rad) and in the latitude range from -156.68° (-2.7346 rad) to -156.43° (-2.7302 rad). The approximate distance is calculated using equations 9 through 11.

$$d = \left(\sqrt{x^2 + y^2}\right) * 2.5X10^{-8} \tag{9}$$

$$x = 69.1 * (\lambda_2 - \lambda_1) \tag{10}$$

$$y = 69.1 * (\Lambda_2 - \Lambda_1) * Cos\left(\frac{\lambda_1}{57.3}\right) \tag{11}$$

Where d (km) represents the distance between the two locations, λ is the latitude in radians, Λ in radians is the longitude, and 2.5 x 10^{-8} converts the distance from miles to kilometers.

Table 1: Latitude and longitude calculations

Lat1 (rad)	Lon1 (rad)	Lat2 (rad)	Lon2 (rad)	X	Y	Dist (km)
1.2448	-2.7333	1.2451	-2.7346	0.0205	-0.0856	0.0941
1.2448	-2.7333	1.2465	-2.7302	0.1170	0.2158	0.2625

The in-situ latitude and longitude range is within ±0.3km of the MMCR location. This close proximity increases the probability that the MMCR and in-situ measurement will represent the same cloud sampling volume.

The in-situ data is then analyzed according to the mini-VIPS processing techniques described above. Next, the particle size and area ratio distributions are extracted and used to calculate the reflectivity according to relationships presented by Heymsfield (1977).

$$Z = \left(\frac{6}{\pi}\right)^2 \times 10^6 \sum_J F(J)A(J) \times \sum_{i=1}^{i\_max} n_i L_i^{2B(J)} \tag{12}$$

$$Z(dBz) = 10\log_{10} Z\left[mm^6 / m^3\right] \quad (13)$$

Where Z ($mm^6\ m^{-3}$) is the reflectivity, $n_i(m^{-3})$ is the number concentration per size bin I, $F(J)$ the fraction of crystals with habit J, L_i the crystal length, and A and B are habit-dependent constants. Lastly, the calculated reflectivity values are averaged over two-minute averages.

Table 2: Mass-length relationships (Heymsfield 1977)

Particle Habit	$A\times10^5$	B	**Data Source**
Bullet Rosettes	4.4	3.0	Heymsfield (1972)
Columns	1.7	1.7	Heymsfield (1972)
Plates	2.6	2.5	Heymsfield (1972)
Water	52	3.0	Heymsfield (1977)

The MMCR radar measures the reflectivity at median points of various altitude ranges. The MMCR radar height levels are shown in the table 3. The reflectivity recorded in the altitude range that corresponds to the aircraft altitude at that same time is extracted for each second within the valid time range. The reflectivity values are then averaged over the same two-minute averages as the in-situ data.

Table 3: MMCR radar height levels

Height Reference	Median Height (m AGL)
0	104
1	194
2	284
3	374
4	464
5	554
6	644
4	734
8	824
9	914
10	1004
11	1094
12	1184
13	1274
14	1364
15	1454
16	1544
14	1634
17	1724
18	1814
19	1904
20	1994

CHAPTER 5

RESULTS AND DISCUSSION

5.1 REFLECTIVITY ANALYSIS

The initial set of results is calculated with the assumption that the habit fraction is 100% column, bullet rosettes, plates, or water. These first approximations are based on the fact that these are the most common shapes seen in mixed-phase and ice clouds (Dowling and Radke 1990; Baker 1997; Macke, Francis et al. 1998; Baran 2004). Table 4 displays the two-minute averages of the calculated and measured reflectivity values. There are some time periods where there are either no radar readings or ice particles are not present on the mini-VIPS video footage. The video footage begins at 21:20:00 UTC.

Table 4: 2-min averages of calculated and measured reflectivity values

Initial Time (UTC)	Columns (dBz)	Bullet Rosettes (dBz)	Plates (dBz)	Water (dBz)	No. of in-situ Frames	MMCR (dBz)	No. of radar Measure - ments
21:20:00	-33.104	-39.818	-38.656	-18.367	81		0
21:22:00	-33.527	-40.318	-39.143	-18.867	95		0
21:24:00	-37.052	-46.680	-44.414	-25.229	70		0
21:26:00	-34.993	-42.823	-41.243	-21.372	94		0
21:28:00	-34.411	-42.014	-40.531	-20.563	91		0
21:30:00	-35.739	-44.158	-42.350	-22.707	101	-36.624	1
21:32:00	-31.729	-37.037	-36.425	-15.586	83	-31.286	4
21:34:00	-34.602	-42.096	-40.640	-20.645	111	-31.576	3
21:48:00	-40.933	-53.377	-50.018	-31.926	77		0
21:50:00	-42.183	-56.077	-52.175	-34.626	91	-24.295	3
21:52:00	-39.932	-51.905	-48.842	-30.583	101	-33.147	3
21:54:00	-40.547	-52.888	-49.164	-30.933	97	-38.014	3
21:56:00	-42.460	-56.424	-52.754	-35.283	117	-28.976	4
21:58:00	-40.015	-51.909	-48.768	-30.458	115	-37.291	1
22:00:00	-37.776	-47.858	-45.409	-26.407	84	-37.063	3

Atlas et al (1995) analyzed in-situ data from the First International Satellite Cloud Climate Climatology Project (ISCCP) Regional Experiment (FIRE I) and concluded that radar reflectivity from cirrus ice particles should range from approximately -50 dBz to +10 dBz. All of the radar reflectivity values reported in table 4 are well within this range. Most of the calculated reflectivity values from all of the habit-based assumptions were also within the range. The bullet rosette calculations do result in some reflectivity values that fall below the lower limit.

The reflectivity calculations from each of these habits are represented in Figures 17 and 18. To compare both data sets the in-situ reflectivity is plotted as a function of the radar reflectivity against the 1:1 line. Values that lie above the 1:1 line indicate a higher in-situ reflectivity value than the cloud radar. Values below the 1:1 line indicate a lower in-situ reflectivity and on the 1:1 line represent equivalent in-situ and radar reflectivity.

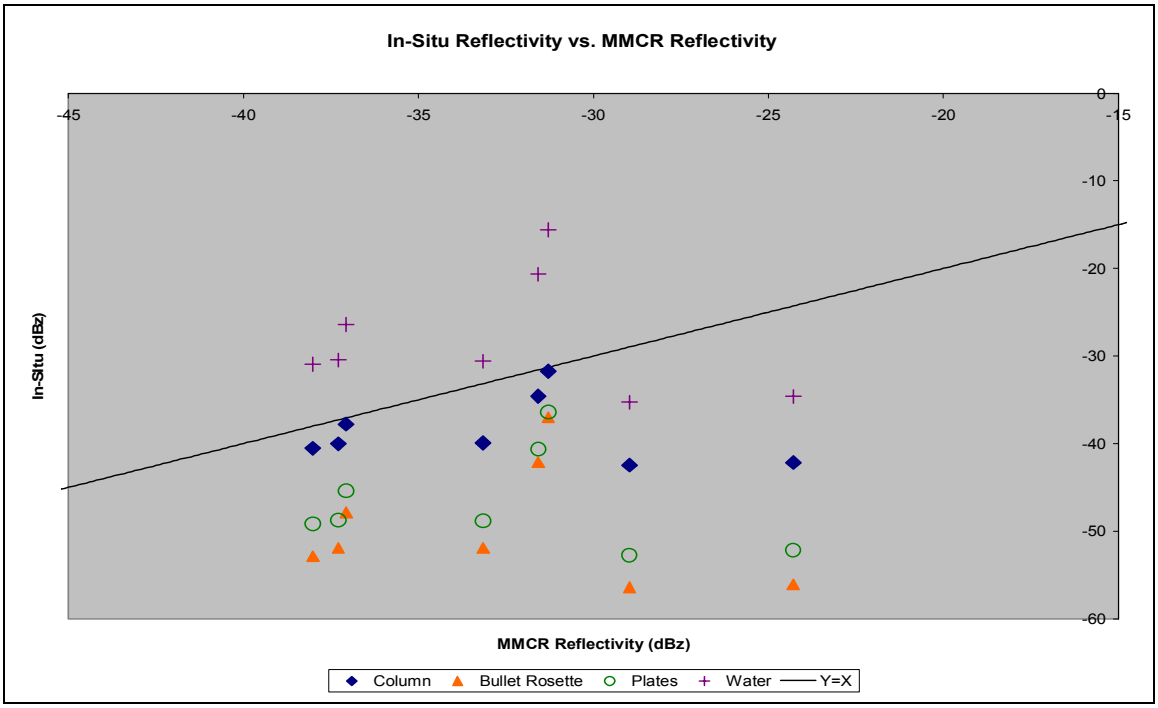

Figure 17: In-situ reflectivity values versus MMCR measurements

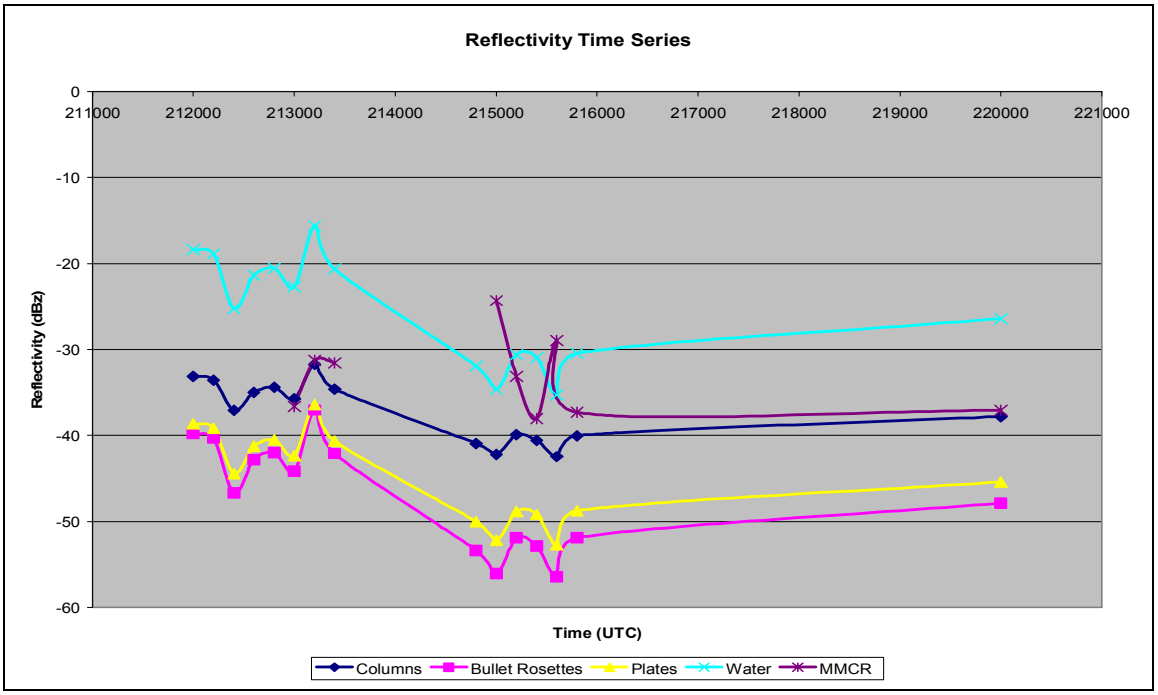

Figure 18: Time series of in-situ and MMCR reflectivity values

It can be seen from figure 17 that the bullet rosettes, plates, and water reflectivity calculations to not correlate well with the ground-based measurements. The column-habit assumption seems to represent a better correlation at some times throughout the observation period. The good correlation with the column assumption calculation is consistent with the shapes seen in the mini-VIPS image processing. The reflectivity time series, figure 18, graphically displays the calculated and measured reflectivity values as a function of time. It can be seen that the columns correlated to the best around the time frame between 21:20:00 UTC and 21:40:00 UTC. At later times, the MMCR reflectivity values were in between column and water calculations. This could be indicative of the presence of a mixed-phase air mass.

Figures 19 displays selected representative frames during the time period where the columns correlated well with the radar reflectivity. Figures 13 shows representative frames selected the time period where the radar values seem to represent a mixed-phase condition.

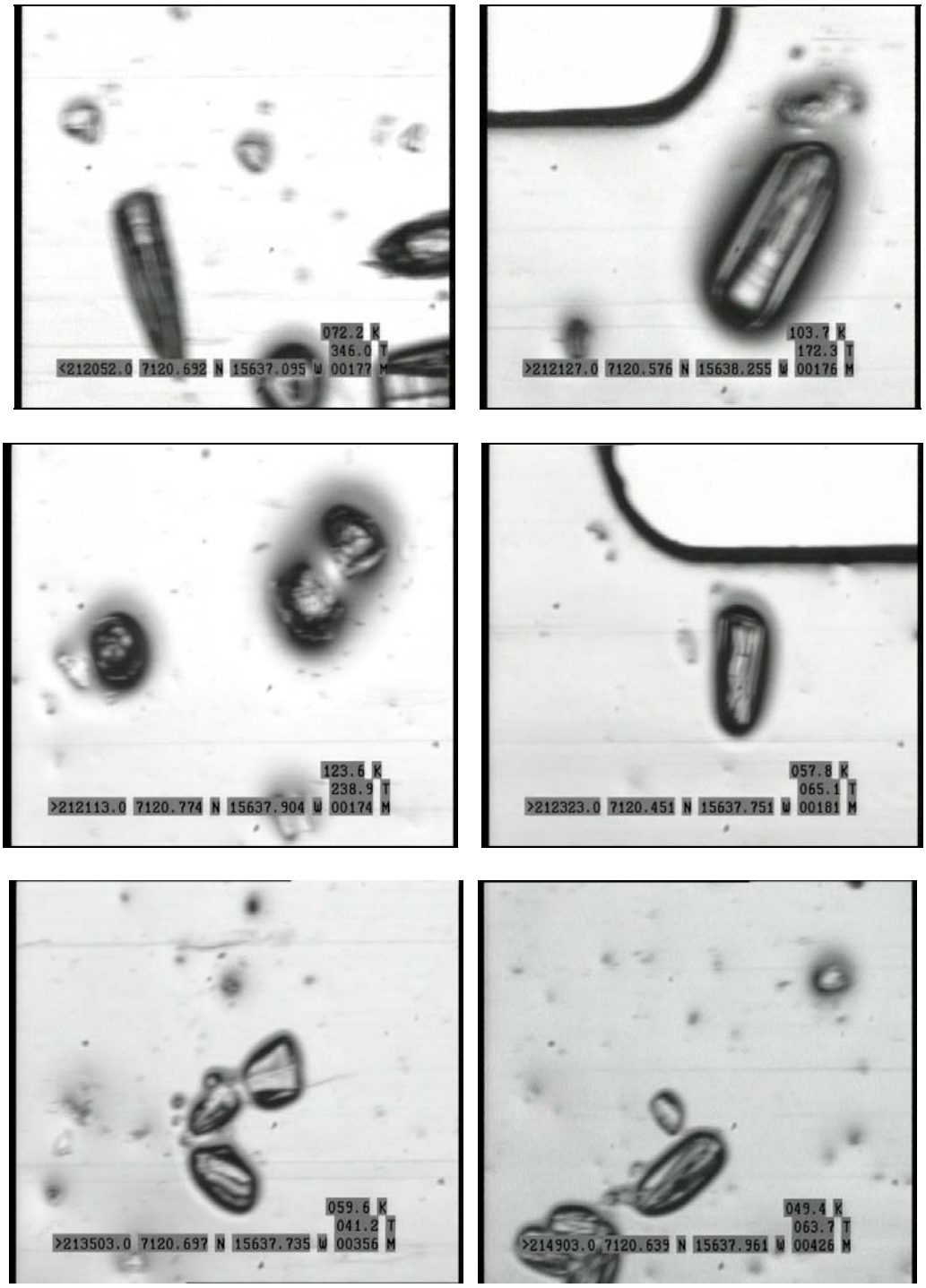

Figure 19: Representative frames during time frame where column-habit calculations have a good correlation

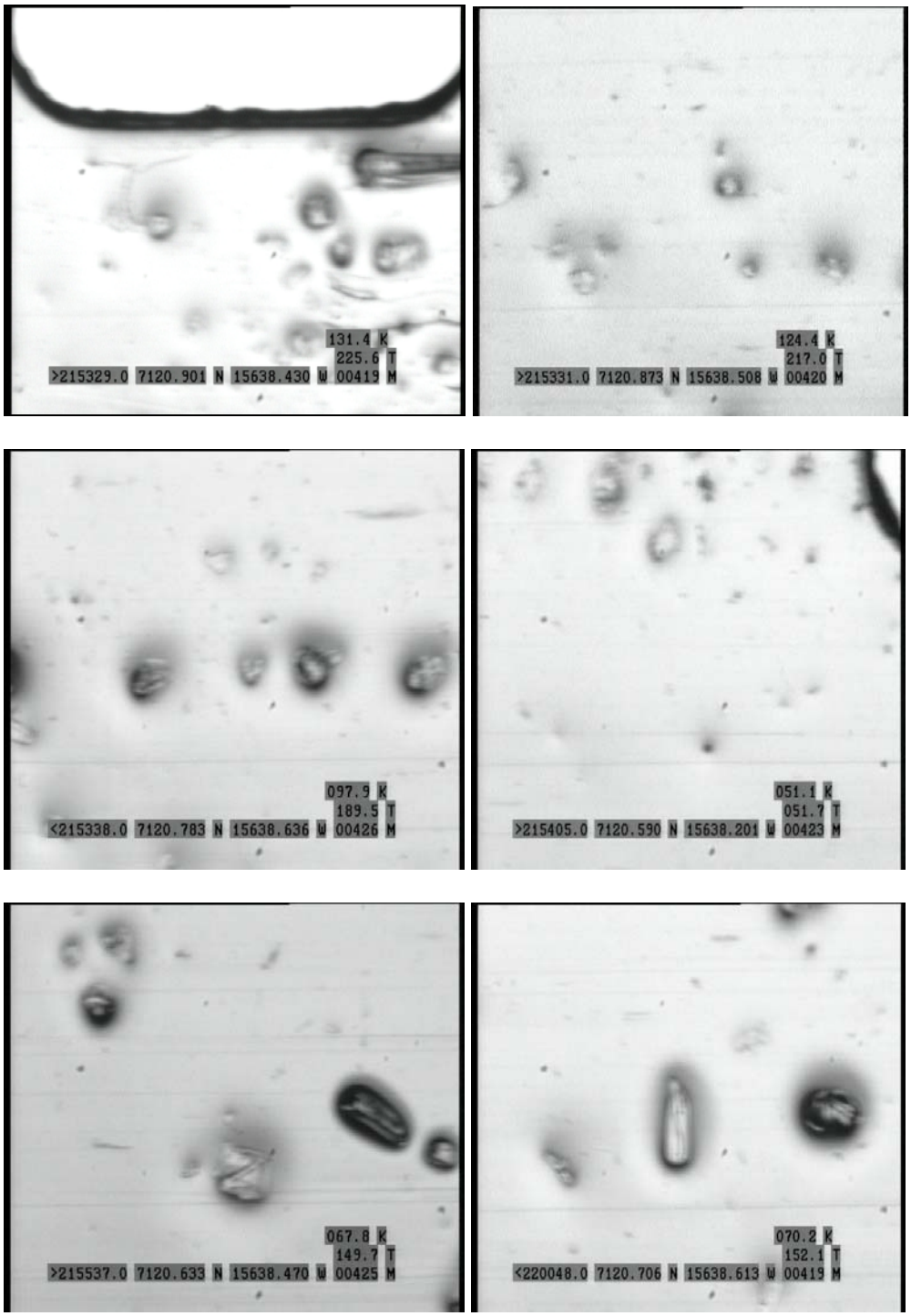

Figure 20: Representative images where the reflectivity correlations were poor

The upper set of frames (figure 19) displays mostly column and quasi-spherical particles. These particles are distinct and can be assumed in good confidence to actually be in the ice phase. Some column-like particles still exist in the second set of frames (figure 19); however, more quasi-spherical particles and particles that appear lighter (or “shallower”) are seen in the lower set of frames. There is a time period between 21:00:00 UTC to 21:51:00 where the sampled volume is saturated with respect to ice according to the relative humidity profile. During the second time frame, the relative humidity profile shows values of between 80% and 90% indicating that the conditions are not conducive to ice formation. These are likely water or evaporated ice particles. Therefore, this change in particles can be attributed to the evaporation of the ice crystals as the sampling volume became less supersaturated with respect to ice. Based on relative humidity with respect to ice profile, the time series, and the representative frames it can be inferred that an ice cloud was not being sampled during this time period

Figures 21 and 22 show extracted data just from the time period where the relative humidity with respect to ice is approximately 100%. The columns calculations correlate very well with the cloud radar measurements. The good correlation during this time period indicates that the particles seen during this time period are probably not water droplets, and are indeed small ice crystals.

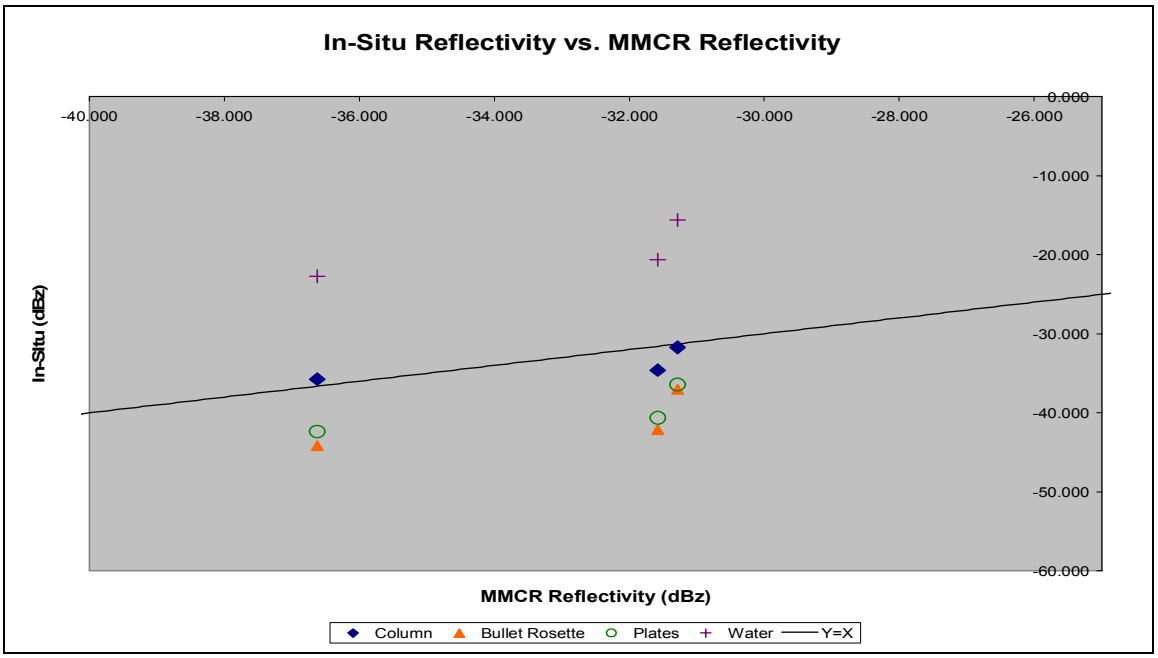

Figure 21: In-situ reflectivity values versus MMCR reflectivity during ice saturation period

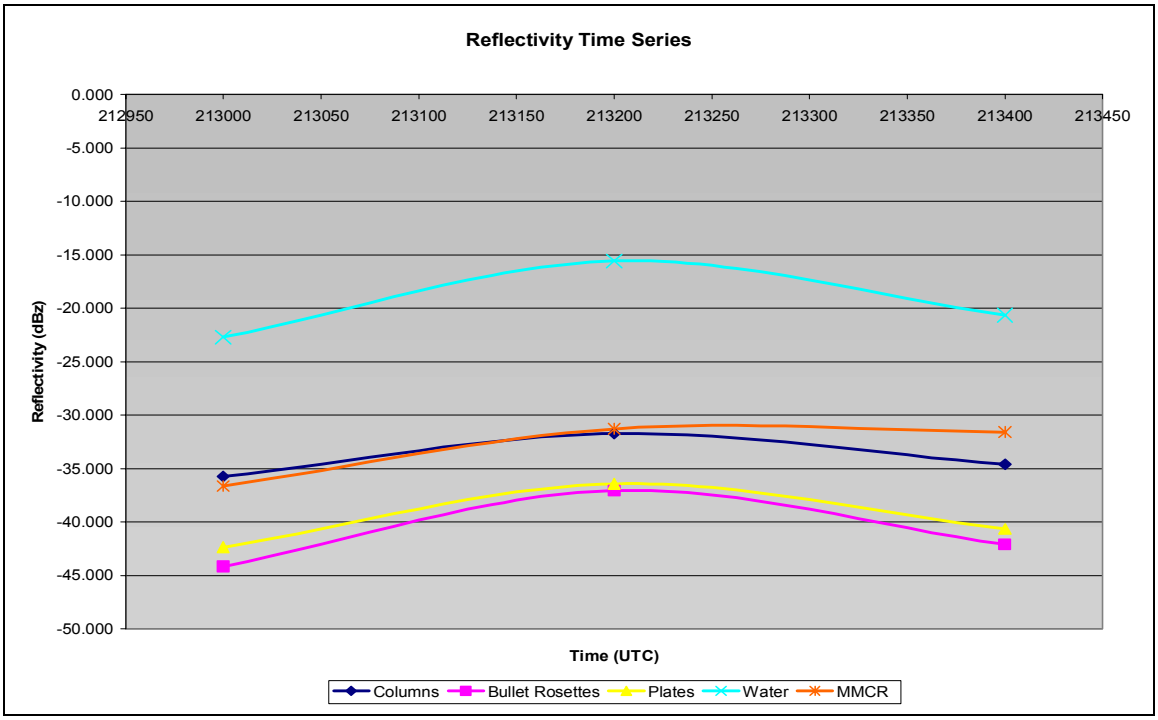

Figure 22: Reflectivity time series from ice saturation time period

5.2 PARTICLE HABIT ANALYSIS

The area ratio distributions can be analyzed to gain more information about particle habit. Heymsfield and Miloshevich (2003) reported area ratio vs. diameter relationships for individual particle habits that were derived from experimental data. The values were related by equation 14.

$$A_r = C_0 \times D^{C1} \tag{14}$$

Where A_r represents the area ratio, C_0, C_1 are habit-dependent constants, and D represents the particle's maximum diameter in cm.

Table 5: Area ratio vs. diameter relationships for individual particles habits (Heymsfield and Miloshevich 2003)

Habit	**C_0**	**C_1**	**Range (μm)**	**Area Ratio Range (eq. 14)**	**No. of Particles**
Columns (Balloon replicator, FIRE-II, cirrus)	0.061	-0.411	90-470	0.422-0.214	416
Single Rosettes (CPI, 9 Mar 2000, cirrus)	0.125	-0.351	100-1000	0.629-0.280	2016
Hexagonal Plates (Heymsfield and Kajikawa; 1987; surface)	0.78	0	26-600	0.78	30

The valid diameter range for all of the habit area ratio correlations described above is a good representation of the in-situ mini-VIPS data particle size distribution range of 0-500μm. Therefore the parameters from table 6 can be used to set reasonable boundaries of the area ratios that are representative of columns, single rosettes, and hexagonal plates. From the calculated corresponding area ratio range, it can be seen that the columns and single rosettes are indistinguishable from each other. However, the hexagonal plates have a higher value and can be distinguished.

Figures 23 shows the averaged area ratio distributions for the two-minute intervals displayed in figure 22. The maximum area ratio value is slightly below 0.3, which is characteristic of columns and single rosettes. However, the particles are smaller than the observed data range from the studies reported in table 6. Therefore, one can conclude that the data range reported in table 6 can be extended to smaller particles. [AN11]

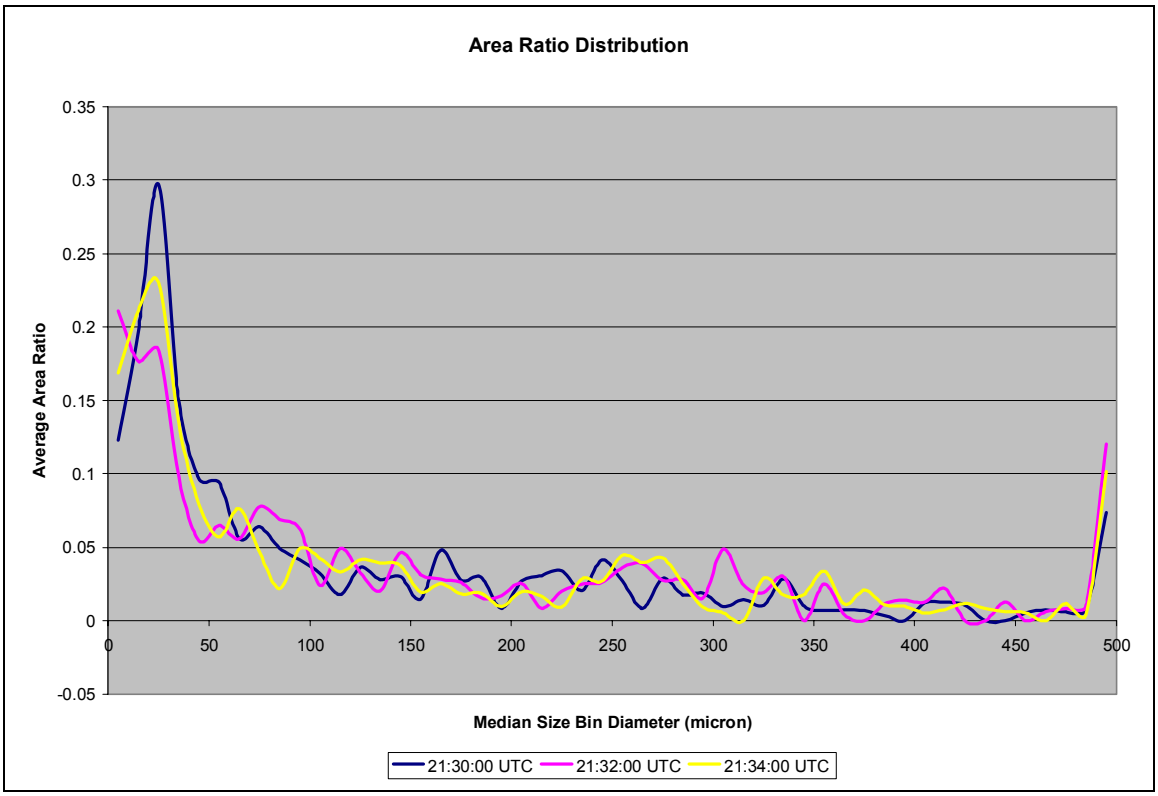

Figure 23: 2-min average area ratio distributions during ice saturation time period

The particle habit is dependent on ambient temperature (hence altitude and season). The different temperatures suggest a specific ice formation process and habit. Therefore, the temperature profile shown in figure 24 and adapted from Heymsfield and Miloshevich (2003) can be used as a standard of comparison the habits seen during our flight mission. The characteristic profiles are samples from the NCAR balloon-borne replicator in a cirrus cloud on 25 Nov 1991, near Coffeyville, KS during the NASA FIRE II Experiment.

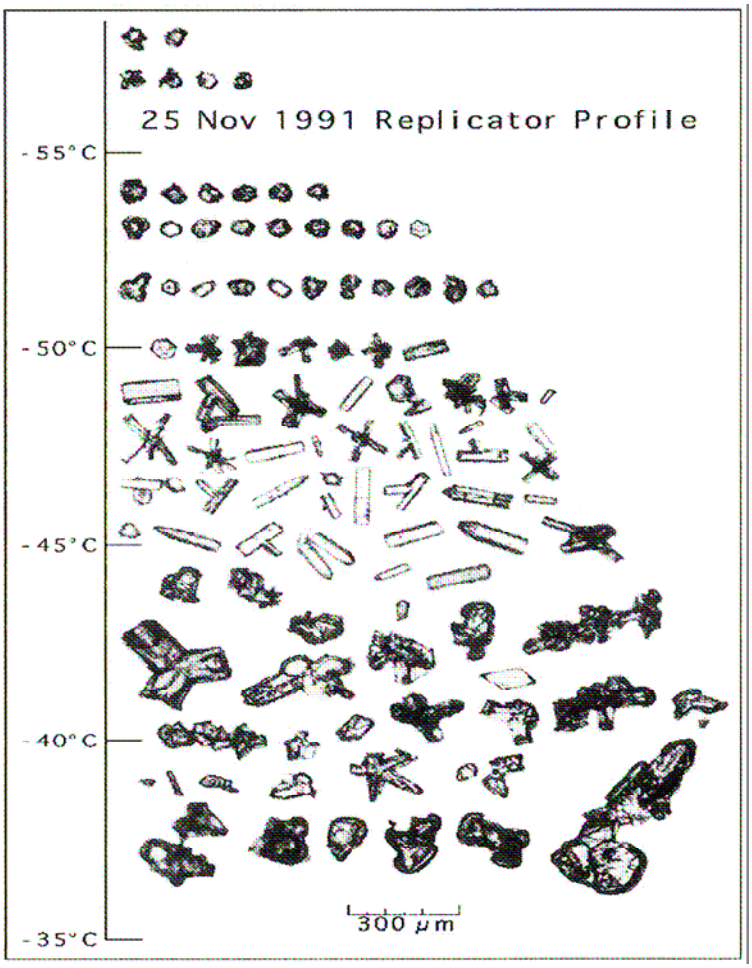

Figure 24: Temperature profile of characteristic ice particles sampled by the NCAR balloon-borne replicator in a cirrus cloud on 25 NOV 1991, near Coffeyville, KS during the NASA FIRE II experiment

The ice particles found at the lower temperatures are more than likely formed by homogenous nucleation or specifically sublimation. These particles tend to be more round. The particles found at higher temperatures are more likely to have been formed by heterogeneous nucleation leading to larger, more open particles (Heymsfield and Miloshevich 2003).

The temperature during our data collection ranged in between -31°C to 35°C. Therefore, our particle habits should be closely related to the habits found at the bottom of the Heymsfield and Miloshevich (2003) temperature profile. Figure 17 shows representative frames from the mini-VIPS data that exhibit these similar habits.

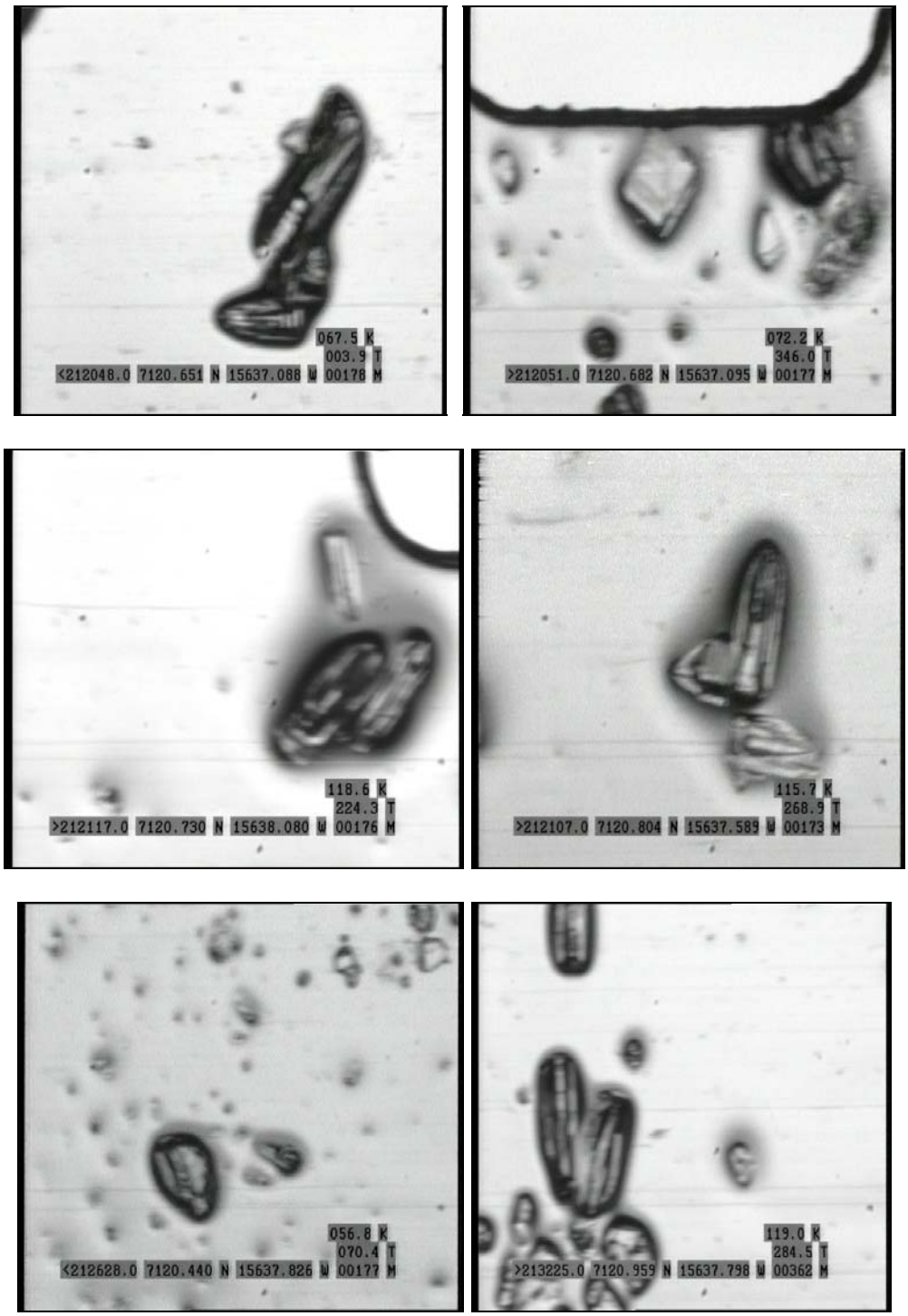

Figure 25: Images from the saturation period that correlate well to the characteristic diagram

The images from the mini-VIPS data seen in figure 25 visually correlate to the characteristic ice particle temperature profile. The fact the this flight temperature is slightly higher than the upper limit on the diagram and the fact that the mini-VIPS data is sampled in a high-latitude area versus the mid-latitude region sampled on the profile may be the source of some discrepancies.

5.3 PARTICLE SIZE ANALYSIS

Radar reflectivity is heavily influenced by particle size; therefore, it is of interest to examine the particle sizes that are present in the ice cloud case. Figure 26 displays the two-minute averaged number distributions from the ice case. The number distribution is clearly dominated by the particle sizes below 100μm (Platt et al. 1989; Dowling and Radke 1990). Dowling and Radke (1990) compares several particle size distributions measured from a variety cirrus types, conditions, and locations and reports the common theme amongst all cases is the fact that large particles are less common than smaller particles. This same theme is seen in figure 26. The smooth curves below 100μm compared to the noisy values at larger diameters suggest that there is greater confidence in the mini-VIPS measurement of the smaller diameter particles.

Figure 27 displays the particle mass distribution for the same time frame. For simplicity, the distribution is calculated assuming that all of the ice particles are spherical and have a density of $0.9168\frac{g}{cm^3}$. In contrast to the particle size

distribution, the larger particles contribute the most to the mass. As a result, these particles play a major role in the reflectivity value. Some of the larger ice particles that are closer to the higher end of the VIPS detection limit could have possible not been captured completely by the mini-VIPS footage possible leading to an underestimation of the in-situ reflectivity value. This phenomenon will have to be further explored.

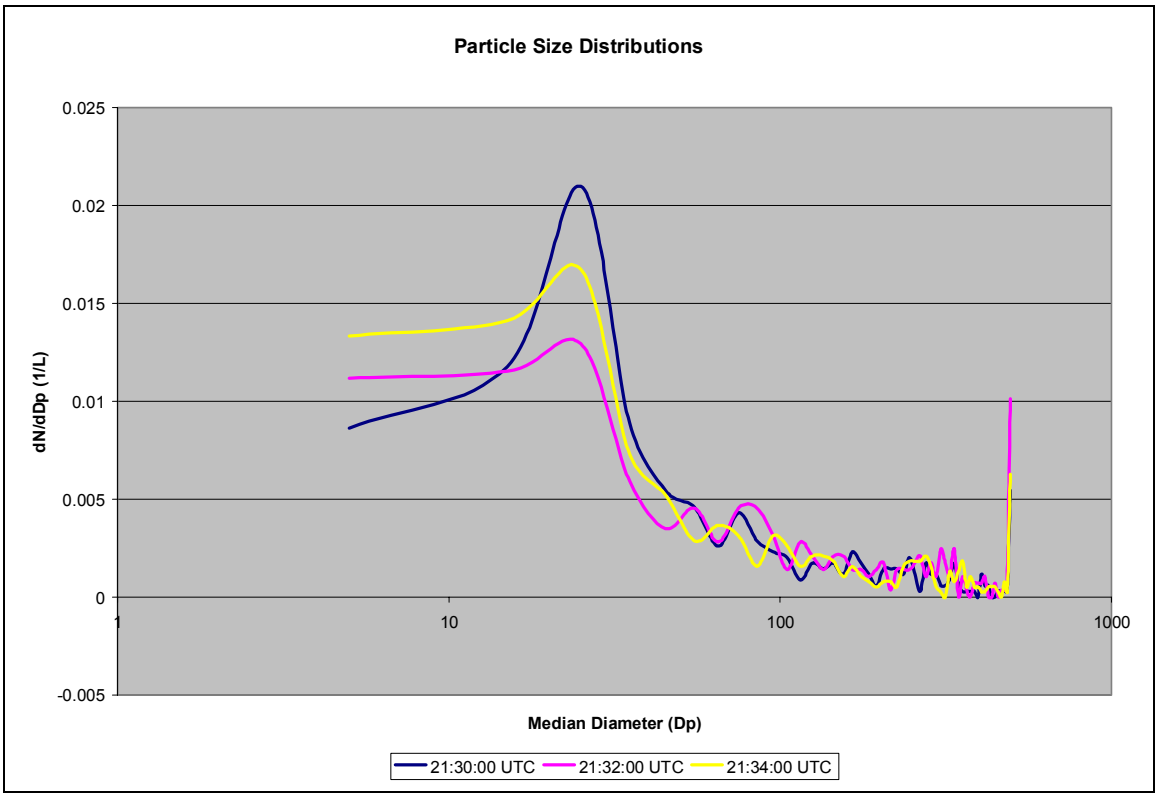

Figure 26: Particle Size Distributions for ice saturation time period

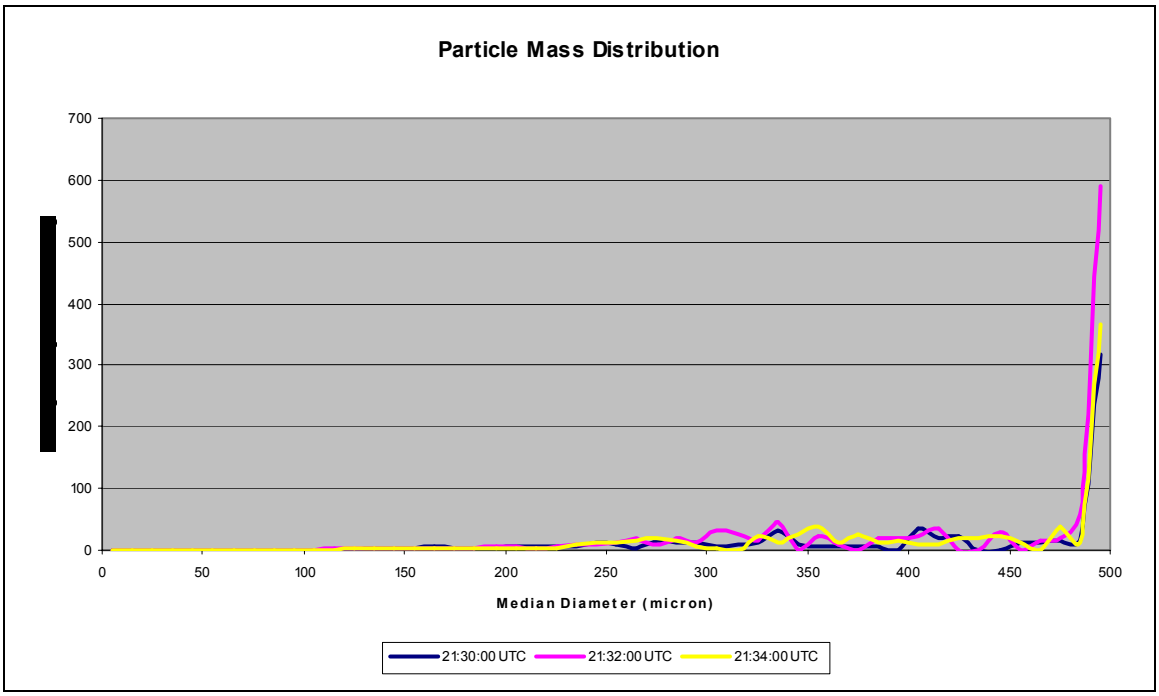

Figure 27: Particle mass distributions during ice saturation time period

CHAPTER 6

SUMMARY, CONCLUSIONS, AND FUTURE DIRECTION

This study is the first of its kind that evaluates the performance of the mini-VIPS against ground-based remote-sensing measurements, for clouds sampled during a flight of the 2004 Artic Operations Program in Barrow, Alaska. The remote sensing platform used in the intercomparison was the millimeter cloud radar operated by ARM/CART at the Barrow site. Specifically, retrieved radar reflectivity values are compared to the reflectivity values calculated using the relationship described by Heymsfield (1977). The sensitivity of the intercomparison with respect to particle habit and size of the sampled clouds were also explored.

An agreement of ±3.06 dBZ between calculated (using the mini-VIPS microphysical data) and the MMCR cloud reflectivity is attained for time periods where the Aerosonde UAV (where the mini-VIPS was located on) was located deep inside the cloudy layers. The closure was best when the “column-shaped” assumption was invoked in the radar calculations, in agreement with the observations from the image analysis. The closure significantly worstened when alternate crystal geometries (i.e., rosette, plates and liquid water droplets) were assumed. The uncertainty of the radar is ±2.00 dBZ; therefore, the agreement seen in this study is only slightly outside of the radar uncertainty range. The good

correlation within the ice saturation cloud case leads to the inference that the mini-VIPS is a reliable and robust platform for in-situ measurements. Thereby, there is an increase in the confidence in mini-VIPS and MMCR data. The validation of these techniques is very promising. Further analysis will lead to greater understanding of the role of smaller ice crystal particles in the radiative properties of mixed-phase and ice clouds. These results also demonstrate the great potential of UAVs as a platform. Inexpensive and less hazardous missions will increase the amount of data that can be collected.

The MMCR reflectivity values correlated better with the calculated water-assumption reflectivity values during some times when the sampled volume was not saturated with respect to ice. This observation can lead to the conclusion that some liquid water could have been present at these very low temperatures. The uniform phase assumption to calculate the in-situ reflectivity values can serve as a base case. However, accounting for co-existing phases within a sampling volume can be used to further investigate the possibility of mixed-phase clouds existing at temperatures as low as -30°C.

The microphysical properties of the sampled clouds were also noted. For the temperatures sampled, ice particle habit and size distributions are similar to trends seen in other latitude regions. It was also seen that the habit area ratio correlations adapted from Heymsfield and Miloshevich (2003) can be utilized for smaller size particles than reported in the literature.

The extension of this work has the potential to lead to other significant findings. The immediate plan is to extend the analysis to larger time periods that

cover not only wintertime conditions, but also summer and fall seasons in the Arctic. This analysis will lead to a more statistically significant sampling, and can further validate the correlation between in-situ mini-VIPS and ground-based data.

Furthermore, one can assess the effects of ambient conditions, especially changes thereof, on the microphysical evolution of the ice clouds. An important issue that remains to be explored is the stability of mixed phase clouds, as the timescale of glaciation of these clouds will be an important factor for their climatic impacts in this sensitive region of the globe. Finally, the potential effects of aerosols on the microphysical evolution (both for liquid phase and ice phase) is at this point completely unknown; the mini-VIPS, in conjunction with remote radar can provide a unique inside on the aerosol indirect effect for these sensitive clouds.

REFERENCES

Albrecht, B. (1989). "Aerosols, cloud microphysics, and fractional cloudiness." Science **245**: 1227-1230.

Arnott, W. P., Y. Dong, et al. (1994). "Role of small ice crystals in radiative properties of cirrus: A case study, FIRE II, November 22, 1991." Journal of Geophysical Research **99**(D1): 1371-1381.

Atlas, D., S. Matrosov, et al. (1995). "Radar and Radiation Properties of Ice Clouds." Journal of Applied Meteorology **34**(11): 2329-2345.

Bailey, M. and J. Hallett (2004). "Growth Rates and Habits of Ice Crystals between -20 C and -70 C." Journal of the Atmospheric Sciences **61**: 514-544.

Baker, M. B. (1997). "Cloud Microphysics and Climate." Science **276**(5315).

Baran, A. J. (2004). "On the Scattering and absorption properties of cirrus cloud." Journal of Quantitative Spectroscopy & Radiative Transfer **89**: 17-36.

Baumgardner, D., H. Chepfer, et al. (2005). "The shapes of very small cirrus particles derived from in-situ data measurements." Geophysical Research Letters **32**: L01806.

Baumgardner, D. and A. V. Korolev (1997). "Airspeed corrections for optical array probe sample volumes." Journal of Atmospheric and Oceanic Technology **14**(5): 1224-1229.

Boucher, O., S. E. Schwartz, et al. (1998). "Intercomparison of models representing direct shortwave radiative forcing by sulfate aerosols." Journal of Geophysical Research - Atmospheres **103**(D14): 16, 979-16,998.

Charlson, R. J., S. E. Schwartz, et al. (1992). "Climate forcing by anthropogenic aerosols." Science **255**: 423-430.

Clothiaux, E. E., M. A. Miller, et al. (2001). The ARM Millimeter Wave Cloud Radars (MMCRs) and the Active Remote Sensing of Clouds (ARCSL) Value Added Product (VAP).

Coakley, J. A., R. L. Bernstein, et al. (1987). "Effect of ship-stack effluents on cloud reflectivity." Science **237**: 1020-1022.

Curry, J. A., E. E. Ebert, et al. (1988). "Mean and Turbulence Structure of the Summertime Arctic Cloudy Boundary-Layer." Quarterly Journal of the Royal Meteorological Society **114**(481): 715-746.

Curry, J. A., J. Maslanik, et al. (2004). "Applications of Aerosondes in the Artic." Bulletin of the American Meteorological Society **85**(12): 1855-1861.

Curry, J. A., W. Rossow, et al. (1996). "Overview of Arctic cloud and radiation characteristics." Journal of Climate **9**(8): 1731-1764.

Dowling, D. R. and L. F. Radke (1990). "A summary of the physical properties of cirrus clouds." Journal of Applied Meteorology **29**: 970-978.

Ebert, E. E. and J. A. Curry (1992). "A parameterization of ice cloud optical properties for climate models." Journal of Geophysical Research **97**: 3831-3836.

Fleishauer, R. P., V. E. Larson, et al. (2002). "Observed Microphysical Structure of Midlevel, Mixed-Phase Clouds." Journal of the Atmospheric Sciences **59**: 1779-1804.

Gardiner, B., D. Lamb, et al. (1985). "Measurements of initial potential gradient and particle charges in a Montana summer thunderstorm." Journal of Geophysical Research-Atmospheres **90**(ND4): 6079-6086.

Garrett, T., P. V. Hobbs, et al. (2001). "Short-wave, single-scattering properties of arctic ice clouds." Journal of Geophysical Research-Atmospheres **106**(D14): 15155-15172.

Gayet, J.-F., F. Auriol, et al. (2002). "Quantitative Measurement of the Microphysical and Optical Properties of Cirrus Clouds with Four Different In-Situ Probes: Evidence of small ice crystals." Geophysical Research Letters **29**(24): 83.

Gerber, H., B. G. Arends, et al. (1994). "New microphysics sensor for aircraft use." Atmospheric Research **32**: 235-252.

Gerber, H., C. H. Twohy, et al. (1998). "Measurements of Wave-Cloud Microphysical Properties with Two New Aircraft Probes." Geophysical Research Letters **25**(8): 1117-1120.

Ghan, S., L. Leung, et al. (1997). "Application of cloud microphysics to NCAR community climate model." Journal of Geophysical Research-Atmospheres **102**(D14): 16507-16527.

Glickman, T., Ed. (2000). Glossary of Meteorology. Boston, MA, American Meteorological Society Press.

Gultepe, I., G. A. Isaac, et al. (2000). "Dynamical and microphysical characteristics of arctic clouds during BASE." Journal of Climate **13**(7): 1225-1254.

Gultepe, I., G. A. Issac, et al. (2003). "Turbulent heat fluxes over leads and polynyas, and their effects on Arctic clouds during FIRE.ACE Aircraft observations for April 1998." Atmospheric-Ocean **41**(1): 15-34.

Haywood, J. and O. Boucher (2000). "Estimates of hte direct and indirect radiative forcing due to tropospheric aerosols: A review." Reviews of Geophysics **38**(4): 513-543.

Haywood, J. and K. P. Shine (1995). "The effect of anthropogenic sulfate and soot on the clear-sky planetary radiation budget." Geophysical Research Letters **22**: 603-606.

Hegg, D. A., R. J. Ferek, et al. (1993). "Light scattering and cloud condensation nucleus activity of sulfate aerosol measured over the northeastern Atlantic Ocean." Journal of Geophysical Research **98**: 14,887-14,894.

Heintzenberg, J. (1989). "Fine particles in th global troposphere A review." Tellus **41**(B): 149-160.

Heymsfield, A., G. M. McFarquhar, et al. (1998). "Cloud properties leading to highly reflective tropical cirrus: Interpretations from CEPEX, TOGA, COARE, and Kwajalein, Marshall Islands." Journal of geophysical Research - Atmospheres **103**(D8): 8805-8812.

Heymsfield, A. J. (1977). "Precipitation Development in Stratiform Ice Clouds: A Microphysical and Dynamical Study." Journal of the Atmospheric Sciences **34**: 367-381.

Heymsfield, A. J., A. Bansemer, et al. (2004). "Effective Ice Particle Densities Derived from Aircraft Data." Journal of the Atmospheric Sciences **61**: 982-1003.

Heymsfield, A. J. and G. M. McFarquhar (1996). "High Albedos of Cirrus in the Tropical Pacific Warm Pool: Microphysical Interpretations from CEPEX and from Kwajalein, Marshal Islands." Journal of the Atmospheric Sciences **53**(17): 2424-2451.

Heymsfield, A. J. and L. M. Miloshevich (2003). "Parameterizations for the Cross-Sectional Area and Extinction of Cirrus and Stratiform Ice Cloud Particles." Journal of the Atmospheric Sciences **60**: 936-956.

Hobbs, P. V., Ed. (1993). Aerosol-Cloud-Climate Interactions. International Geophysics Series. San Diego, California, Academic Press, Inc.

Holland, G. J., J. A. Curry, et al. (2001). "The Aerosonde robotic aircraft: A new paradigm for environmental observations." Bulletin of the American Meteorological Society **82**(5): 889-901.

Hollars, S., Q. Fu, et al. (2004). "Comparison of cloud-top height retrievals form ground-based 35 GHz MMCR and GMS-5 satellite observations at ARM TWP Manus site." Atmospheric Research **72**(1-4): 169-186.

Houghton, D. D., R. Gallimore, et al. (1991). "Stability and variability in a coupled ocean-atmosphere climate model - results of 100-year simulations." Journal of Climate **4**(6): 557-577.

Houghton, J. T., Y. Ding, et al., Eds. (2001). Climate Change 2001: The Scientific Basis. Contribution of Working Group I to the Third Assessment Report of the Intergovernmental Panel on Climate Change. United Kingdom and New York, NY, USA, Cambridge University Press.

Isaac, G. A. and R. A. Stuart (1996). "Relationships between cloud type and amount, precipitation, and surface temperature in the Mackenzie River Valley-Beaufort Sea area." Journal of Climate **9**(8).

Jacob, D. J. (1999). Introduction to atmospheric chemistry. Princeton, New Jersey, Princeton University Press.

Khvorostyanov, V. I. and K. Sassen (1998). "Cirrus Cloud Simulation Using Explicit Microphysics and Radiation. Part I: Model Description." Journal of the Atmospheric Sciences **55**: 1808-1821.

King, M. D., S. Platnick, et al. (2004). "Remote sensing of liquid water and ice cloud optical thickness and effective radius in the Arctic: Application of airborne multispectral MAS data." Journal of Atmospheric and Oceanic Technology **21**(6): 857-875.

Kinne, S., T. Ackerman, et al. (1992). "Cirrus Microphysics and Radiative Transfer - Cloud Field-Study on 28 October 1986." Monthly Weather Review **120**(5): 661-684.

Lawson, R., A. V. Korolev, et al. (1998). "Improved measurements of the drop size distribution of a freezing drizzle event." Atmospheric Research **48**: 181-191.

Lawson, R. P., B. A. Baker, et al. (2001). "An overview of microphysical properties of Arctic clouds observed in May and July 1998 during FIRE ACE." Journal of Geophysical Research **106**(D14): 14989-15014.

Leaitch, W. R., G. A. Isaac, et al. (1992). "The relationship between cloud droplet number concentrations and anthropogenic pollution: Observations and climatic implications." Journal of Geophysical Research **97**: 2463-2474.

Lohmann, U. and J. Feichter (2004). "Global indirect aerosol effects: a review." **4**: 7561-7614.

Macke, A., P. N. Francis, et al. (1998). "The Role of Ice Particle Shapes and Size Distributions in the Single Scattering Properties of Cirrus Clouds." Journal of the Atmospheric Sciences **55**: 2874-2883.

Marchand, R., T. Ackerman, et al. (2001). "Multiangle observations of Arctic clouds from FIRE ACE: June 3, 1998, case study." Journal of Geophysical Research-Atmospheres **106**(D14): 15201-15214.

Martin, G. M., D. W. Johnson, et al. (1994). "The measurement and parameterization of effective radius of droplets in warm stratiform clouds." Journal of the Atmospheric Sciences **51**: 1823-1842.

Matrosov, S. Y., A. J. Heymsfield, et al. (1995). "Ground-Based Remote Sensing of Cloud Particle Sizes during the 26 November 1991 FIRE II Cirrus Case: Comparsions with In Situ Data." Journal of the Atmospheric Sciences **52**(23): 4128-4142.

Matrosov, S. Y., A. J. Heymsfield, et al. (1998). "Comparisons of Ice Cloud Parameters Obtained by Combined Remote Sensor Retrievals and Direct Methods." Journal of Atmospheric and Oceanic Technology **15**: 184-196.

McFarquhar, G. M. and S. G. Cober (2004). "Single-scattering properties of mixed-phase Arctic clouds at solar wavelengths: Impacts on radiative transfer." Journal of Climate **17**(19): 3799-3813.

McFarquhar, G. M. and A. Heymsfield (1997). "Parameterization of tropical cirrus ice crystal spectra and implications for radiative transfer: Results from CEPEX." Journal of the Atmospheric Sciences **54**: 2187-2201.

McFarquhar, G. M. and A. J. Heymsfield (1996). "Microphysical Characteristics of Three Anvils Sampled During the Central Equatorial Pacific Experiment." Jornal of the Atmospheric Sciences **53**(17): 2401-2423.

McFarquhar, G. M., A. J. Heymsfield, et al. (1999). "Use of Observed Ice Crystal Sizes and Shapes to Calculate Mean-Scattering Properties and Multispectral

radiances: CEPEX April 4, 1993, case study." Journal Of Geophysical Research **104**(D24): 31763-31779.

McGill, M., L. Li, et al. (2004). "Combined lidar-radar remote sensing: Initial results from CRYSTAL-FACE." Journal of Geophysical Research-Atmospheres **109**(D7).

Meehl, G. and W. Washington (1990). "CO2 Climate Sensitivity and Snow-Sea-Ice Albedo Parameterization in and Atmospheric GCM Coupled to A Mixed-Layer Ocean Model." Climatic Change **16**(3): 283-306.

Mitrescu, C., J. Haynes, et al. (2005). "Cirrus cloud optical, microphysical, and radiative properties observed during the CRYSTAL-FACE experiment: A lidar-radar retrieval system." Journal of geophysical Research - Atmospheres **110**(D9).

Moran, K. P., B. E. Martner, et al. (1998). "An Unattended Cloud-Profiling Radar for Use in Climate Research." Bulletin of the American Meteorological Society **79**(3): 443-455.

Nemesure, S., R. Wagener, et al. (1995). "Direct shortwave forcing of climate by anthropogenic sulfate aerosol: Sensitivity to particle size, composition, and relative humidity." Journal of Geophysical Research **100**): 26,105-26,116.

Noone, K., K. Noone, et al. (1993). "In-Situ observations of cirrus cloud microphysical properties using the counterflow virtual impactor." Journal of Atmospheric and Oceanic Technology **10**(3): 294-303.

Novakov, T., C. Riveria-Carpio, et al. (1994). "The effect of anthropogenic sulfate aerosols on marine cloud droplet concentrations." Tellus **46**: 132-141.

Penner, J. E., R. E. Dickinson, et al. (1992). "Effects of aerosol from biomass burning on the global radiation budget." Science **256**: 1432-1434.

Pilinis, C., S. N. Pandis, et al. (1995). "Sensitivity of direct climate forcing by atmospheric aerosols to aerosol size and composition." Journal of Geophysical Research **100**: 18,739-18,754.

Platt, C. M. R., J. D. Spinhirne, et al. (1989). "Optical and Microphysical Properties of a Cold Cirrus Cloud - Evidence for Regions of Small Ice Particles." Journal of geophysical Research - Atmospheres **94**(D8): 11151-11164.

Pryzybylak, R. (2003). The Climate of The Arctic. Boston, MA, Kluwer Academic Publishers.

Radke, L. F., J. A. Coakley, et al. (1989). "Direct and remote sensing observations of the effects of ships on clouds." Science **246**: 1146-1149.

Ranson, Jon. "What are Aerosols?" NASA. 2004 <http://terra.nasa.gov/FactSheets/Aerosols>

Seinfeld, J. H. and S. N. Pandis (1998). Atmospheric Chemistry and Physics: From Air Pollution to Climate Change, John Wiley & Sons.

Shupe, M. and J. Intrieri (2004). "Cloud radiative forcing of the Arctic surface: The influence of cloud properties, surface albedo, and solar zenith angle." Journal of Climate **17**(3): 616-628.

Shupe, M., T. Uttal, et al. (2001). "Cloud water contents and hydrometeor sizes during the FIRE Arctic Clouds Experiment." Journal of Geophysical Research-Atmospheres **106**(D14): 15015-15028.

Stokes, G. M. and S. E. Schwartz (1994). "The Atmospheric Radiation - Measurement (ARM) Program - Programmatic Background and Design of the Cloud and Radiation Test-Bed." Bulletin of the American Meteorological Society **75**(7): 1201-1221.

Strapp, J. W., F. Albers, et al. (2001). "Laboratory measurements of the response of a PMS OAP-2DC." Journal of Atmospheric and Oceanic Technology **18**(7): 1150-1170.

Strom, J. and J. Heintzenberg (1994). "Water-Vapor, Condensed Water, and Crystal Concentration in orographically influenced cirrus clouds." Journal of the Atmospheric Sciences **51**(16): 2368-2383.

Takano, Y. and K. Liou (1989). "Solar radiative-transfer in cirrus clouds. 1. Single-Scattering and optical properties of hexagonal ice crystals." Journal of the Atmospheric Sciences **46**(1): 3-19.

Turner, D. (2005). "Arctic mixed-phase cloud properties from AERI lidar observations: Algorithm and results from SHEBA." Journal of Applied Meteorology **44**(4): 427-444.

Twohy, C., A. Schanot, et al. (1997). "Measurement of condensed water content in liquid and ice clouds using an airborne counterflow virtual impactor." Journal of Atmospheric and Oceanic Technology **14**(1): 197-202.

Vali, G. (1999). Ice Nucleation - Theory: A Tutorial. NCAR/ASP 1999 Summer Colloquium.

Villa, J. M., S. L. Cruz-Pol, et al. (2002). Modeling, Simulation, and Comparison Study of Cirrus Clouds' Ice Crystals. Mayaguez, Puerto Rico Amherst, Massachusetts, University of Puerto Rico

Microwave Remote Sensing Laboratory**:** 9.

Wang, Z. and K. Sassen (2002). "Cirrus Cloud Microphysical Property Retrieval Using Lidar and Radar Measurements. Part I: Algorithm Description and Comparison with In Situ Data." Journal of Applied Meteorology **41**: 218-229.

Warren, S., C. Hahn, et al. (1985). "Simultaneous Occurrence of Different Cloud Types." Journal of Climate and Applied Meteorology **24**(7): 658-667.

Wigley, T. (1991). "Could reducing fossil-fuel emissions cause global warming." Nature **349**(6309): 503-506.

Wilson, L. D., J. A. Curry, et al. (1993). "Satellite Retrieval of Lower-Tropospheric Ice Crystal Clouds in the Polar-Regions." Journal of Climate **6**(7): 1467-1472.

Wyser, K. and C. G. Jones (2005). "Modeled and observed clouds during Surface Heat Budget of the Arctic Ocean (SHEBA)." Journal of geophysical Research - Atmospheres **110**(D9).

Zhang, T., K. Stamnes, et al. (1996). "Impact of clouds on surface radiative fluxes and snowmelt in the arctic and sub-Arctic." Journal of Climate **9**(9): 2110-2123.

Zuidema, P., B. A. Baker, et al. (2005). "An arctic springtime mixed-phase cloudy boundary layer observed during SHEBA." Journal of the Atmospheric Sciences **62**(1): 160-176.